

## CHAPTER 5

# The low-frequency dielectric properties of biological cells

Christopher L. Davey and Douglas B. Kell\*

*Institute of Biological Sciences, University of Wales, Aberystwyth, Dyfed, UK*

- 1 Introduction
- 2 Theory of the dielectric experiment
  - 2.1 The concepts of impedance and admittance
  - 2.2 Intrinsic system properties: permittivity, conductivity and dielectric relaxation
- 3 Mechanisms of dielectric dispersion in biological systems
- 4 Mechanisms of dielectric relaxation in cell suspensions and tissues
  - 4.1 Overview
  - 4.2 The  $\alpha$ -dispersion
  - 4.3 The  $\beta$ -dispersion
  - 4.4 Membrane properties and the  $\beta$ -dispersion
- 5 Nonlinear interactions of cells with electrical fields
- 6 A four state enzyme capable of harvesting electrical energy for the performance of useful (bio)chemical work
- 7 Concluding remarks
- Acknowledgments
- References
- Appendix A. Glossary

## 1. Introduction

The passive electrical or "dielectric" properties of biological cells have been studied since the last century [1]. Important advances in our knowledge that have accrued from the application of dielectric spectroscopy to biological systems include the recognition of the molecular thickness of biological membranes [2] and of the existence of voltage-gated ion channels as embodied in the Hodgkin-Huxley [3] equations. However, as judged by its complete omission from a book on *Biological Spectroscopy* [4], the technique has not achieved as widespread a recognition and exploitation in biophysics as it warrants [5]. Notwithstanding, and due in large part to advances in instrumentation which make the acquisition, display and interpretation of biological dielectric spectra much more convenient than has historically been the case, the

\*To whom correspondence should be addressed.

last 10 or 15 years have seen a significant increase in the use of the technique [5-18a].

Our scope in this chapter is therefore as follows. First, we shall outline the direct methods used to measure the low-frequency dielectric properties of biological materials, and give an outline of the relevant theory of biological and other dielectrics. After this the linear, low-frequency dielectric properties of cell suspensions are considered in detail. Lastly, the nonlinear dielectric properties of biological materials are considered, along with the potential applications of this branch of dielectrics.

## 2. Theory of the dielectric experiment

### 2.1. The concepts of impedance and admittance

In this section we describe the means by which one obtains a direct estimation of the dielectric properties of biological (or other) systems. Somewhat more indirect methods such as electrorotation and dielectrophoresis, through which one may also infer the dielectric properties of biological cells, in some cases in more detail, are described *in extenso* in chapter 6.

The generalised dielectric experiment may be described with reference to Fig. 1. In this, a small-amplitude, sinusoidally modulated current  $I = I_m \sin \omega t$ , of frequency  $\omega$  radians  $s^{-1}$  ( $\omega = 2\pi f$ , where  $f$  is the frequency in Hz), is applied to the system of interest. In the (quasi-) steady state, after any transients have died down, a potential difference is generated across the system with a time-dependence or waveform  $U = U_m \sin(\omega t - \theta)$ , where  $\theta$  is known as the phase angle (Fig. 1). Provided that the system is linear in the sense that the potential difference generated is proportional to the current flowing, the current and the potential difference are sinusoids of the same frequency, and the dielectric properties are uniquely determined by the macroscopic observables  $U_m$ ,  $I_m$  and  $\theta$ .

For present purposes, the system under test may be taken to behave (at a given frequency) either as a resistor ( $R'$ ) and capacitor ( $C'$ ) in series or as a conductor ( $G$ ) and capacitor ( $C$ ) in parallel. Both models are equally valid and it is considerations of the convenience in handling the mathematics and the actual measurements which dictates which is used. Thus dielectric spectroscopy provides a clear separation between the experimenter and the system under test, and may indeed be viewed as the "archetypal" black box approach in which the properties of a system of interest are inferred from its measured response to a known stimulus.

Physically, one way to consider the relationship between the phase angle and the magnitudes of the resistance and capacitance in the

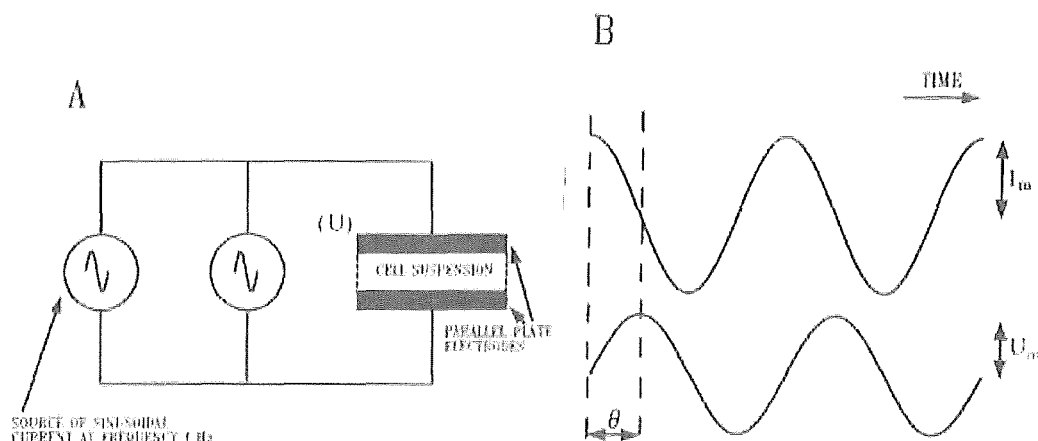


Fig. 1. A dielectric measurement in which a sinusoidally modulated a.c. current of amplitude  $I_m$  is applied to the system of interest, in this case a cell suspension. The result of this is that a potential difference  $U$  (amplitude  $U_m$ ) of the same frequency, phase shifted by an amount ( $\theta$  radians) which reflects the macroscopic capacitance and conductance of the suspension, is generated across the system. For a pure capacitor the current leads the potential difference by  $\pi/2$  radians, whilst for a pure resistor current and potential difference are exactly in phase. (A) Generalised measurement system. (B) Waveforms of potential difference and current; the modulus of the impedance is the ratio  $U_m/I_m$  and the modulus of the admittance is the ratio of  $I_m/U_m$ .

system is to begin with the fact that all of the energy in the exciting electrical field must either be stored (as a capacitive term) or dissipated (as a resistive term), and that storage takes time whilst dissipation to heat is instantaneous on the time-scale of present interest. The result of this is that for a pure resistor the phase angle is zero. However, if the system under test is a pure capacitor the current leads the potential difference by  $\pi/2$  radians; in other words, the potential difference is  $90^\circ$  out-of-phase with the current. Real biological systems, at a given frequency, behave as a resistor and capacitor in series (or parallel), so that the phase angle takes a value between zero and  $90^\circ$ .

Impedances and admittances are complex, vector quantities (in the sense that they contain both real and imaginary parts). The impedance is given by  $Z = R' + iX$  where  $R'$  is the resistance,  $X$  the reactance

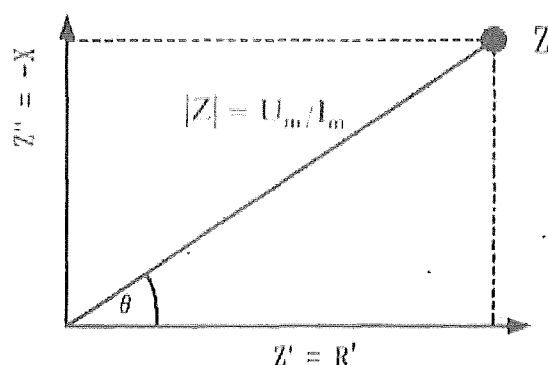


Fig. 2. Impedance is a complex quantity, containing both real and imaginary parts. The modulus of the impedance and the phase angle are used to obtain the resistance ( $R'$ ) and reactance ( $X$ ) according to the relations  $R' = |Z| \cos \theta$  and  $X = -|Z| \sin \theta$ .

( $= -1/\omega C'$ ) and  $i = (-1)^{1/2}$ . The relationship between  $Z$ ,  $U_m$ ,  $I_m$  and  $\theta$  is given in Fig. 2.  $|Z|$  is known as the modulus of the impedance and  $\theta$  the argument. From simple trigonometrical consideration it is evident that  $R' = |Z| \cos \theta$ ,  $X = -|Z| \sin \theta$  and  $Z^2 = R'^2 + X^2$ . The units of  $Z$ ,  $R'$  and  $X$  are ohms ( $\Omega$ ) whilst the SI unit for capacitance is the farad (F). The admittance  $Y$  is the reciprocal of the impedance (i.e.,  $Y = (1/Z) = (G + iB)$ ) where  $G$  is the conductance and  $B (= \omega C)$  the susceptance of the system. The units of  $Y$ ,  $G$  and  $B$  are siemens (S). It is obvious that since these concepts of impedance, admittance, conductance, resistance, susceptance and reactance are only different ways of treating the system under test, they must be related to each other in some way; Table 1 groups together the relevant relationships.

Whilst any linear system may be treated, at a given frequency, as consisting of a resistor and capacitor in series or in parallel, regardless of the actual complexity of the equivalent electrical circuit, it is only possible to distinguish the appropriate equivalent electrical circuit if the frequency is varied. Indeed, it is because one studies the absorption by the system of electrical energy (electromagnetic radiation) *as a function of frequency* that the technique is indeed a form of spectroscopy, variously referred to as Dielectric Spectroscopy [10], Impedance Spectroscopy [19] or Admittance Spectroscopy [12]. Plots of the imaginary part of the impedance or admittance versus the real part (with frequency as the parameter) tend to give semicircles, each semicircle corresponding to a capacitive element in the admittance domain and with the time constant  $\tau$  given by  $RC$  (which has units of s).

## 2.2. Intrinsic system properties: permittivity, conductivity and dielectric relaxation

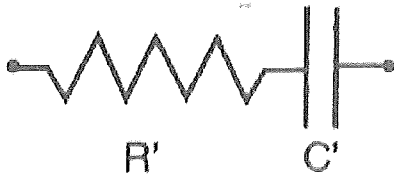
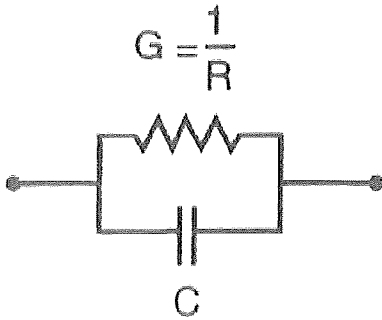
If the system studied consists of a cell suspension connected to the measuring device via two plane-parallel electrodes, the currents measured in response to an exciting voltage will depend upon the area  $A$  of each electrode and the separation  $d$  between them. The intrinsic properties of the system held between the electrodes are the conductivity  $\sigma'$  and the relative permittivity  $\epsilon'_r$ , which are related respectively to the observable admittance domain conductance  $G$  and capacitance  $C$  by

$$\epsilon'_r = Cd/(A\epsilon_0) \quad (1)$$

$$\sigma' = G(d/A) \quad (2)$$

where  $\epsilon_0$ , usually known as the "permittivity of the free space", is the capacitance of a unit cell containing a vacuum, and equal to  $8.854 \times 10^{-12}$  F/m. The quantity  $\sigma'$  has units of  $S \cdot m^{-1}$ , but  $\epsilon'_r$  is the permittivity of the material relative to that of a vacuum and is therefore dimensionless. The

Table 1. The relationships between impedance ( $Z$ ) and admittance ( $Y$ ), and their respective real and imaginary parts. The electrical properties of the system as a whole unit can be described (at a given frequency) by "lumping" all its capacitive properties into a single equivalent capacitance component and "lumping" all its resistive properties into a single equivalent resistance component. There are two alternative arrangements for these equivalent "lumped" components, either in series or in parallel. The arrangement chosen will effect the values of each component. In the impedance domain the system is modelled by a capacitor ( $C'$ ) and resistor ( $R'$ ) in series whilst in the admittance domain the equivalent circuit is a capacitor ( $C$ ) and conductor ( $G$ , where  $G = 1/R$ ) in parallel. One uses these simple circuits to describe the electrical properties of the test system as a whole (at a given frequency) irrespective of the actual complexity of the system. One should note that only when the reactance ( $X$ ) or susceptance ( $B$ ) are zero does one get  $R' = (1/G) = R$  and that  $C'$  and  $C$  are not usually equal. In reality the test system may actually be made up of (or modelled by) a network of resistors and capacitors which is frequently fairly complicated, where each electrical component is (usually) frequency independent and each component models a physically meaningful process. By changing the frequency applied to the test system and recording how the "lumped" components  $R'$  and  $C'$  or  $G$  and  $C$  change one can back-calculate the values of the physically meaningful resistance and capacitance terms in the detailed model of the system. At the top of the table the impedance and admittance are defined in terms of the electrical components in their own domains (i.e., in terms of  $R'$  and  $C'$  or  $G$  and  $C$ ). In the lower two rows of the table the impedance domain resistance ( $R'$ ) and reactance ( $X$ ) are defined in terms of the equivalent admittance domain components and the admittance domain conductance ( $G$ ) and susceptance ( $B$ ) are defined in terms of the equivalent impedance domain terms. Thus measurements taken in the impedance domain can be converted to their equivalent admittance domain values (at the same frequency) and vice versa.

Impedance Domain	Admittance Domain
Impedance	Admittance
$Z = 1/Y = R' + iX$ , where $X = \frac{-1}{\omega C'}$	$Y = 1/Z = G + iB$ , where $B = \omega C$ and $G = \frac{1}{R}$
	
Resistance $R' = \frac{G}{G^2 + \omega^2 C^2}$	Conductance $G = \frac{R'}{R'^2 + X^2}$
Reactance $X = \frac{-\omega C}{G^2 + \omega^2 C^2}$	Susceptance $B = \frac{-X}{R'^2 + X^2}$

factor  $d/A$  is known as the cell constant and has the dimension length<sup>-1</sup>. Water at 25°C has a relative permittivity of some 78.4, so it may be calculated from Eqn. 1 that a unit cell containing it has a capacitance of some 6.94 pF.

The relative permittivity ( $\epsilon'_r$ ) reflects the ease with which localised electric charge in the material can be polarised by the application of an electric field, whilst the conductivity reflects the ease with which free electric charges can migrate through the material under the influence of the electric field [20]. In the case of the dielectric properties of biological cell suspensions, the conductivity is normally dominated by the movement of inorganic ions, and reflects the concentration of the ions, their valency and their mobilities.

As with impedance and admittance, one may define a complex relative permittivity  $\epsilon_r^* = \epsilon'_r - i\epsilon''_r$ , which has both real ( $\epsilon'_r$ ) and imaginary ( $\epsilon''_r$ ) parts. The quantity  $\epsilon'_r$  is the permittivity already discussed, and reflects the electrical energy stored by the system, whilst  $\epsilon''_r$  is known as the dielectric loss and reflects the energy dissipated by the system.

The permittivity ( $\epsilon'_r$ ) and conductivity ( $\sigma'$ ) of biological (or other) systems generally changes as a function of the frequency, typically between high- and low-frequency "plateau" values. As the frequency is increased, the permittivity decreases whilst conductivity increases. These changes in the dielectric properties of a material are called dispersions. A substance whose passive electrical behavior is that of a parallel RC circuit, having a single relaxation time, obeys the Debye equation (Fig. 3)

$$\epsilon_{tot}^* = \epsilon'_{th} + \Delta\epsilon'_r(1 + i\omega\tau) \quad (3)$$

where  $\Delta\epsilon'_r = \epsilon'_{cl} - \epsilon'_{th}$ .

$$\epsilon'_{tot} = \epsilon'_{th} + \Delta\epsilon'_r/(1 + \omega^2\tau^2) \quad (4)$$

and

$$\epsilon''_{tot} = \Delta\epsilon'_r(\omega\tau)/(1 + \omega^2\tau^2) \quad (5a)$$

$$= (\sigma'_{\infty} - \sigma'_i)/(2\pi f\epsilon_0) \quad (5b)$$

Here  $\epsilon'_{cl}$  and  $\epsilon'_{th}$  are the limiting relative permittivities at frequencies low and high with respect to the dispersion. The quantity  $\tau$  is the time constant for the dispersion and reflects the time for the electrical (charge) polarisations to occur in the material. It is related to the critical (characteristic) frequency  $f_c$  of the dispersion by  $\tau = 1/(2\pi f_c)$ . The  $f_c$  of dispersion is the frequency when the fall in permittivity (or rise in conductivity) is half completed, i.e., the frequency at which  $\epsilon'_{tot} = \epsilon'_{th} + (\Delta\epsilon'_r/2)$ . These terms are related to the shape of the permittivity and conductivity dispersion plots in Fig. 4.

The magnitude of the change in conductivity ( $\Delta\sigma'$ ) corresponding to a given dispersive fall in permittivity, is given, for the Debye equations,

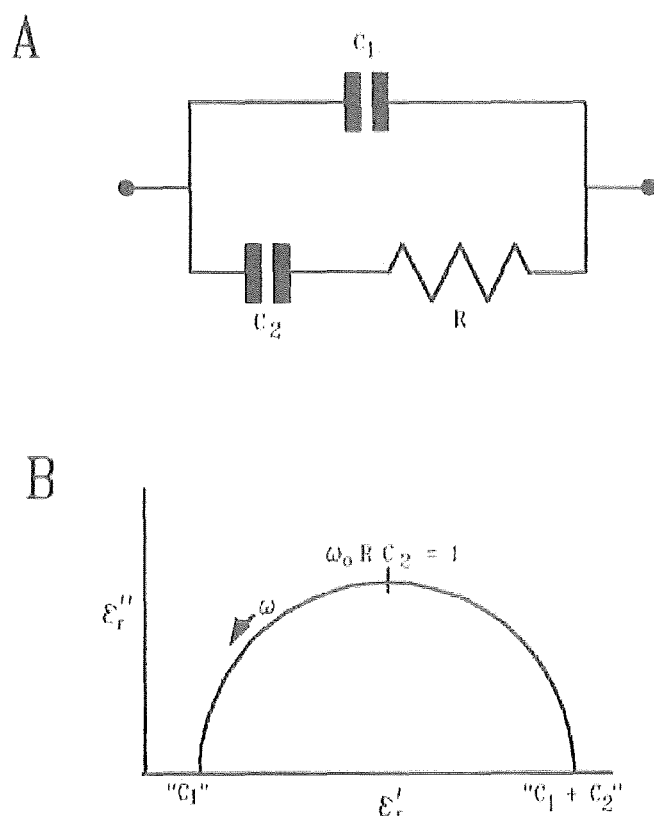


Fig. 3 (A) An equivalent electrical circuit for a substance having but a single relaxation time, such as a system exhibiting Debye behaviour. (B) A complex permittivity plot of the dielectric data obtained therefrom. " $C_1$ " and " $C_2$ " indicate the  $\epsilon'_i$  values arising from  $C_1$  and  $C_2$  according to Eqn. 1

by

$$\Delta\sigma' = (\Delta\epsilon'_i \epsilon_0) / \tau \quad (6)$$

It is clear from this equation that permittivity and conductivity cannot vary independently from each other and that the measurement of one allows (for systems obeying the so-called Kramers-Kronig relationship) the calculation of the other. The other point to notice is that the size of  $\Delta\sigma'$  for a given  $\Delta\epsilon'_i$  depends on the relaxation time of the dispersion. Thus a given  $\Delta\epsilon'_i$  will have a larger corresponding  $\Delta\sigma'$  as the relaxation time decreases, i.e. as its  $f_c$  increases.

Figure 5 is a plot of the variation in  $\epsilon'_i$  and  $\epsilon''_i$  as a function of frequency for a dispersion for which  $\Delta\epsilon'_i = 200$ ,  $f_c = 1$  MHz and  $\epsilon'_{\text{th}} = 80$ , calculated using Eqns. 4 and 5. It is seen that  $\epsilon''_i$  exhibits a peak at the  $f_c$  of the dispersion (in this case 1 MHz). If one plots the values of  $\epsilon''_i$  in Fig. 5 against their equivalent  $\epsilon'_i$  values (using frequency as the parameter), one gets a semicircular graph (Fig. 6). This diagram is called the Cole-Cole [21] or complex permittivity plot, and traces out an

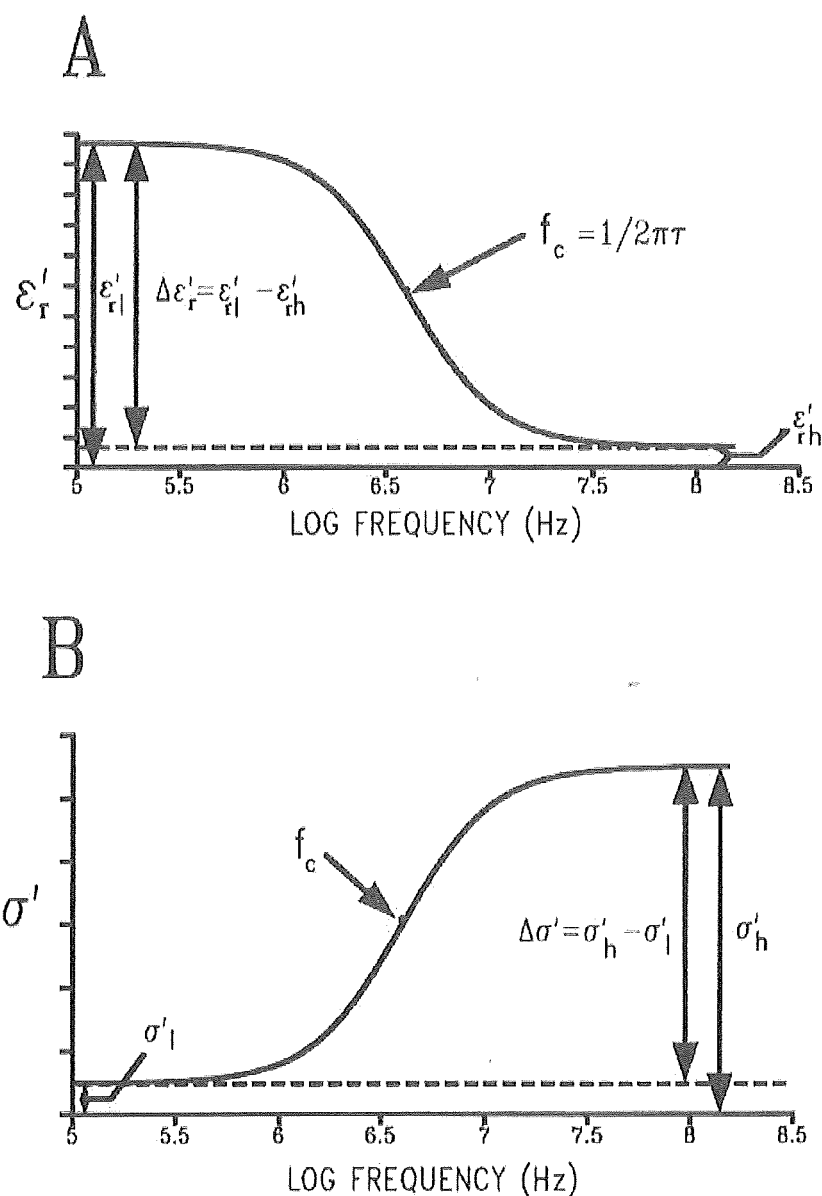


Fig. 4. The changes in relative permittivity ( $\epsilon'_r$ ) and conductivity ( $\sigma'$ ) with frequency are characterised by the values of  $\epsilon'_r$  and  $\sigma'$  before the dispersion has started ( $\epsilon'_{rl}$ ,  $\sigma'_{l}$ ) and after it is complete ( $\epsilon'_{rh}$ ,  $\sigma'_{h}$ ), the size of the changes ( $\Delta\epsilon'_r$  and  $\Delta\sigma'$ ) and the frequency at which  $\Delta\epsilon'_r$  and  $\Delta\sigma'$  are half completed ( $f_c$ ). The effects of frequency on  $\epsilon'_r$  and  $\sigma'$  are shown respectively in (A) and (B).

are obeying the formula

$$(\Delta\epsilon'_r/2)^2 = [\epsilon'_{ro} - (\epsilon'_{rh} + \Delta\epsilon'_r/2)]^2 + (\epsilon''_{ro})^2 \quad (7)$$

Formulae of this structure correspond to the general equation for a (semi)circle, namely  $\text{radius}^2 = (x - h)^2 + (y - k)^2$ . The radius of the semicircle must therefore be  $\Delta\epsilon'_r/2$  and its centre will have the coordinates of  $((\epsilon'_{rh} + \Delta\epsilon'_r/2), 0)$  [8, 22]. As negative values of  $\epsilon'_r$  are physically



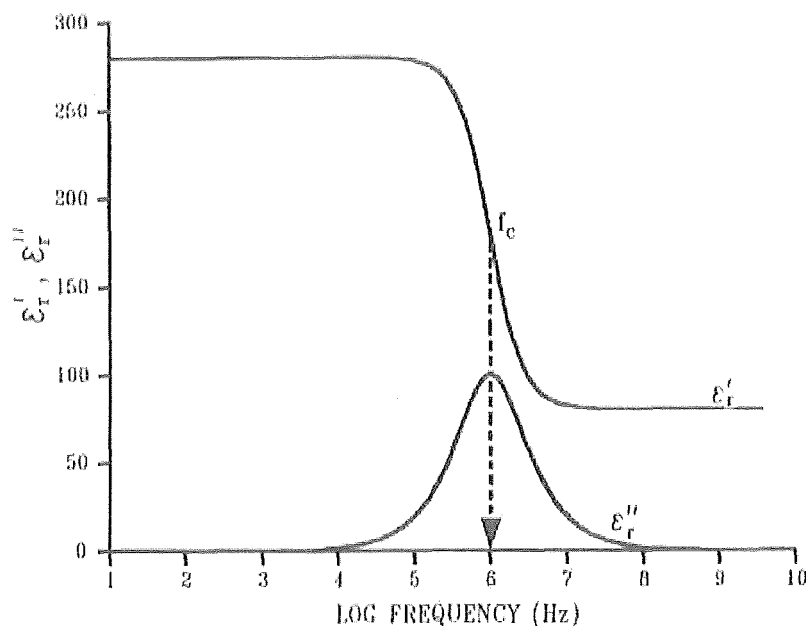


Fig. 5. The change in  $\epsilon'_r$  and  $\epsilon''_r$  with frequency for a dispersion simulated using Eqns. 4 and 5. The values used for the calculation were:  $\Delta\epsilon'_r = 200$ ,  $f_c = 1$  MHz and  $\epsilon'_{rh} = 80$ . The  $\epsilon'_r$  values pass from a low to a high frequency plateau as frequency is increased whilst the  $\epsilon''_r$  curve exhibits a peak at the  $f_c$  of the dispersion.

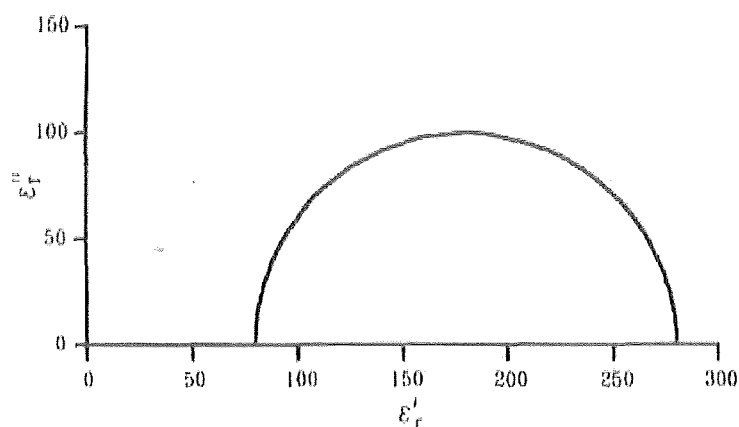


Fig. 6. A complex permittivity, or Cole-Cole plot, of the data in Fig. 5. As seen, the locus of the points forming the data is a semicircle which has its centre on the abscissa.

disallowed for purely dissipative systems, the Cole-Cole plot is usually displayed with positive  $\epsilon''_r$  values only.

In practice, real systems give semicircles whose centres lie below the abscissa, according to an empirical modification of the Debye equation due to the Cole brothers [21]

$$\epsilon_{r\omega}^* = \epsilon'_{rh} + \Delta\epsilon'_r / [1 + (i\omega\tau)^{1-\alpha}] \quad (8)$$

This equation is widely used in biological work, with the coefficient  $\alpha$  ( $0 \leq \alpha < 1$ ), called Cole-Cole  $\alpha$ , usually being taken to reflect some type of distribution of relaxation times, though we would stress that other interpretations are possible [23–25]. A value for  $\alpha$  of 0 implies that there is no distribution of relaxation times (i.e., that there is a single relaxation time) and corresponds to a Debye process. As with the Debye equations one can separate the real and imaginary components yielding new equations for  $\epsilon'_r$  and  $\epsilon''_r$ :

$$\epsilon'_{rw} = \Delta\epsilon'_r [1 + (\omega\tau)^{1-\alpha} \sin(0.5\alpha\pi)] / [1 + 2(\omega\tau)^{1-\alpha} \sin(0.5\alpha\pi) + (\omega\tau)^{2-2\alpha}] + \epsilon'_{rh} \quad (9)$$

$$\epsilon''_{rw} = \Delta\epsilon'_r [(\omega\tau)^{1-\alpha} \cos(0.5\alpha\pi)] / [1 + 2(\omega\tau)^{1-\alpha} \sin(0.5\alpha\pi) + (\omega\tau)^{2-2\alpha}]. \quad (10)$$

The effect of increasing  $\alpha$  on the dispersion given in Fig. 5 is shown in Fig. 7, where increases in  $\alpha$  are reflected in a reduction in the steepness of the fall in  $\epsilon'_r$  with increasing frequency and in a broadening and lowering of the  $\epsilon''_r$  peak. In neither case is the  $f_c$  moved by increasing the value of  $\alpha$ . Similarly, as  $\alpha$  increases the centre of the semicircles on the Cole-Cole plot move further below the abscissa (Fig. 7C).

Certainly the fit of data to Eqn. (9) is generally very good, but as pointed out nearly 40 years ago by Schwan [26], a great many relaxation-time distributions give behaviour virtually indistinguishable from each other (and from the rather complex distribution of relaxation times implicit in the Cole-Cole equations [21, 27]). In other words, the use of  $\alpha$  as a free variable permits one to fit the equation to most data obtained in biological work, regardless of the physical mechanisms at work. Jonscher, Dissado and Hill [23–25] in particular have argued that the wide distribution of relaxation times commonly observed in work with solid-state systems is better ascribed to a *hierarchical interaction* of the relaxing particles with the matrix in which they are embedded, and have proposed an alternative and highly successful fitting function. This seems much more reasonable biologically, since in enzymology it is well known that the functional linkage between enzyme macrostates implies that proteins make transitions between different conformational macrostates *sequentially* and not independently [28–30].

Irrespective of the distribution of relaxation times present, for all linear and many nonlinear dispersive systems, there are general relationships between  $\epsilon'_r$  and  $\epsilon''_r$ , known as the Kramers-Kronig relations (see, e.g., refs. 8, 11, 22, 23, 31). These relations mean that the electrical energy stored (as reflected by  $\epsilon'_r$ ) is always related to the energy dissipated (as reflected by  $\epsilon''_r$ ). In general, the value for  $\epsilon'_r$  at a given frequency depends on the complete area under the  $\epsilon''_r$  spectrum. Similarly, the value of  $\epsilon''_r$  at a given frequency depends on the whole area under the  $\epsilon'_r$  dispersion. An

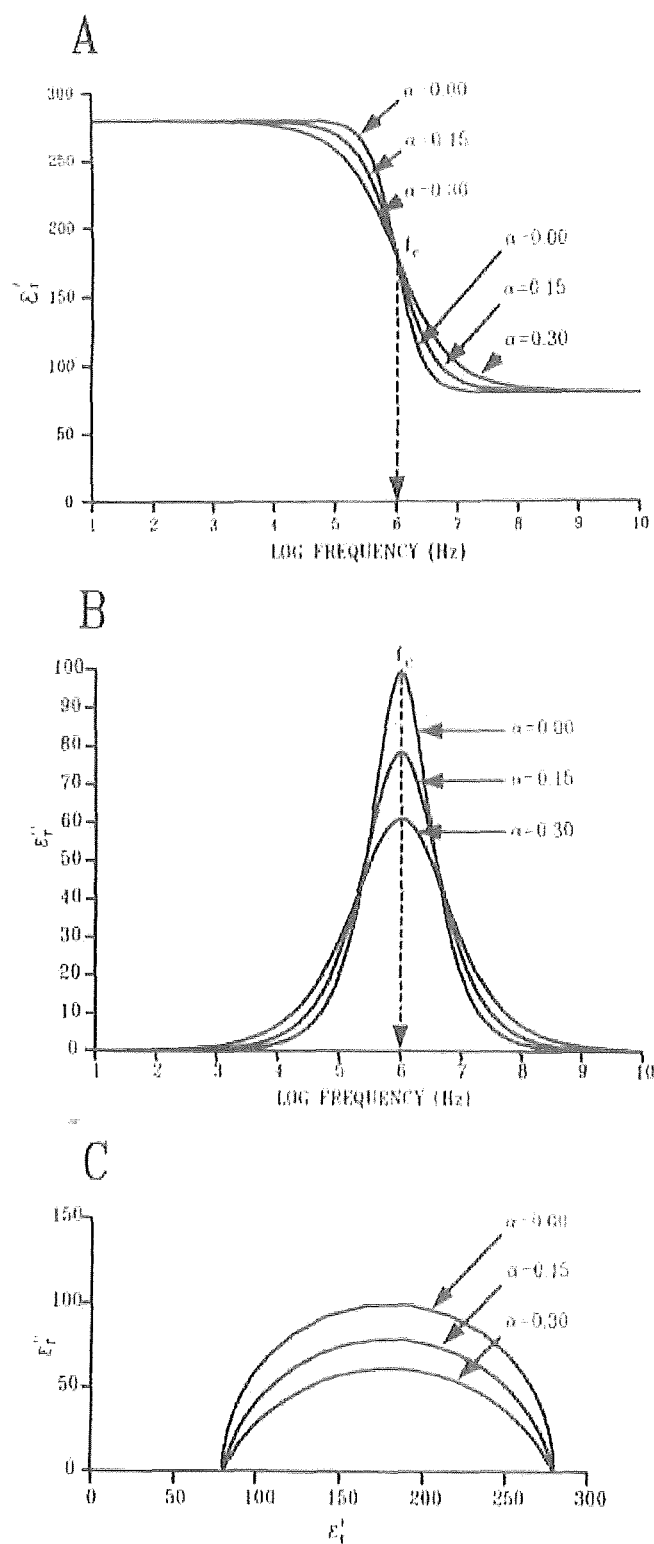


Fig. 7. The effect of a distribution of relaxation times on the data shown in Figs. 5 and 6. The Cole-Cole  $\alpha$  value is zero when there is but one relaxation time (i.e., a Debye process) and increases as the distribution of relaxation times does. As  $\alpha$  increases the slope of the fall in  $\epsilon'_1$  with increasing frequency decreases (A). The effect of increasing  $\alpha$  on the  $\epsilon''_1$  plot is to lower and broaden the peak (B) whilst the result when plotted in the complex permittivity domain is to move the centres of the semicircular plots further and further below the abscissa (C).

exception to this rule is the Debye system where  $\epsilon'_r$  at a given frequency depends only on the  $\epsilon''_r$  at the same frequency [22]. The relationship between energy storage and loss also means that when a fall in  $\epsilon'_r$  occurs during a dispersion then there must be a corresponding increase in  $\sigma'$  (i.e. energy dissipation), and this finds expression in the relationship between the dielectric increment, conductivity increment, and relaxation time for a Debye process given in Eqn. 6.

A further consequence of a distribution of relaxation times (i.e.,  $0 < \alpha < 1$ ) is that the critical frequencies of the fall in permittivity,  $f_{c,\epsilon}$ , and the rise in conductivity,  $f_{c,\sigma}$ , no longer occur at the same frequency. In fact,  $f_{c,\sigma}$  is always greater than  $f_{c,\epsilon}$ . This follows from the superpositioning of Debye processes with different  $f_c$  values, as illustrated in Fig. 8. In Fig. 8A two Debye dispersions of  $\Delta\epsilon'_r = 1000$ ,  $f_c = 100$  kHz and  $\epsilon'_{rb} = 0$ , are superpositioned (i.e., added together). The frequency dependence of the  $\epsilon'_r$  data for each dispersion were calculated using Eqn. 4. The  $\Delta\sigma'$  values corresponding to each fall in  $\epsilon'_r$  were then calculated using Eqn. 6, and the frequency-dependence of  $\sigma'$  was then calculated using the Debye equation for conductivity (with  $\sigma'_i = 0$ ):

$$\sigma'_\omega = \sigma'_i + \Delta\sigma'(\omega^2\tau^2)/(1 + (\omega^2\tau^2)) \quad (11)$$

After this the two permittivity and conductivity plots were superpositioned. As expected, Fig. 8A shows that the superpositioning of two identical dispersions results in no difference between the  $f_c$  values of the conductivity and permittivity curves.

Figure 8B represents data similar to those in Fig. 8A, except that the  $f_c$  value of one of the dispersions was 100 kHz whilst that of the other was 300 kHz. The ratio of the two values of  $\tau$  was 1:3 and, according to Grant et al. [6], using sophisticated deconvolution software, one should *just* be able to distinguish two such overlapping dispersions as separate entities, rather than as a single dispersion with a distribution of relaxation times. Thus, this ratio of  $\tau$  values provides a convenient upper limit to a distribution of relaxation times. To see the effect of this "distribution" of  $f_c$  values on the dispersion data, the calculations were repeated as above, except that the appropriate  $f_c$  values were used. This time (Fig. 8B) the  $f_{c,\sigma}$  is greater than the  $f_{c,\epsilon}$ , just as one finds with real dispersions, even though visually one cannot deconvolute the two underlying dispersion curves. The shift of  $f_{c,\sigma}$  to higher frequencies is a consequence of Eqn. 6.

As was mentioned above, the  $\Delta\sigma'$  corresponding to a given  $\Delta\epsilon'_r$  increases as the  $f_c$  of the dispersion increases. This means that if one has a distribution of  $f_c$  values then the "high- $f_c$ " dispersions in  $\epsilon'_r$  contribute disproportionately large  $\Delta\sigma'$  terms to the resulting superpositioned conductivity curve. The net result of this is that the conductivity curve

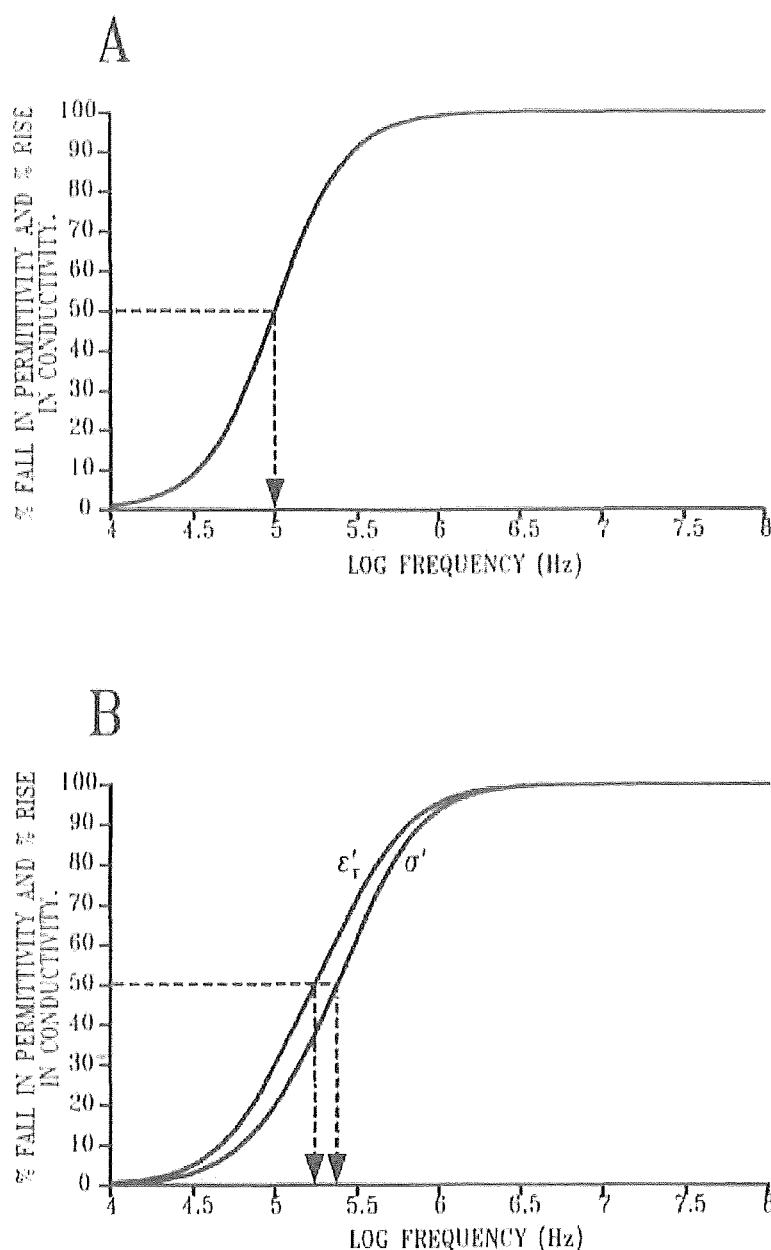


Fig. 8. The effect a distribution of relaxation times has on the characteristic (critical) frequencies of the  $\epsilon'_r$  and  $\sigma'$  plots made up by a superposition of Debye processes. See text for details on how the simulation was performed. (A) The superpositioning of two identical Debye dispersions gives a resultant dispersion with the same characteristic frequency ( $f_c$ ) for both the  $\epsilon'_r$  and  $\sigma'$  curves. (B) Superpositioning two Debye dispersions with differing  $f_c$  values causes the resulting  $\epsilon'_r$  and  $\sigma'$  traces to have different  $f_c$  values. The  $f_c$  value of the  $\sigma'$  data is always higher than that of the equivalent net  $\epsilon'_r$  curve.

becomes biased towards higher frequencies and so its  $f_c$  becomes greater than the mean  $f_{c,\epsilon}$ . As  $f_{c,\sigma}$  is sensitive to the high- $f_c$  components in the distribution of  $f_c$  for  $\epsilon'_r$ , one may expect to obtain a better understand-

ing of the underlying distribution of relaxation times by taking into account both the  $\epsilon'_r$  and  $\sigma'$  data.

### 3. Mechanisms of dielectric dispersion in biological systems

The simplest molecular mechanism underlying a dielectric dispersion [32] is that of the rotation of a molecule, such as a protein, with a permanent (electric) dipole moment  $\mu$ , where we imagine (Fig. 9) that an ensemble of such molecules is held between two electrodes connected to an a.c. source. If this dipole consists of single elementary charges ( $Q^+$ ,  $Q^-$ ) of opposite sign separated by a distance  $s$ , the molecular dipole moment  $\mu$ , which is an intensive property, is given by  $\mu = Qs$ , with units of C m. (For historical reasons, dipole moments are often given in the non-SI unit Debye (D), where  $1 \text{ D} = 3.33 \times 10^{-30} \text{ C m}$ , and the displacement of a single electronic charge through  $10^{-10} \text{ m}$  gives a dipole moment of 4.8 D.) Proteins typically have permanent dipole moments of a few hundred D [33], equal to some 3–5 elementary charges separated by the molecular diameter [17, 34].

If a sinusoidally modulated electrical field is applied to the protein, using a pair of electrodes (equivalent to the plates of a capacitor), the protein will attempt to rotate so that the negative charge is facing the positive electrode and vice versa. Because the net charge on the protein is zero, no d.c. electrophoresis is possible. If the frequency of the field is "low", the protein will have time to orient, and this will be accompanied by a displacement current. When the direction of the field is reversed the protein will reorient to face the opposite electrode. Under these conditions the oriented dipoles of the protein solution result in a net positive charge next to the negative electrode and an equal and opposite charge next to the positive electrode. This charge next to the electrodes then neutralises some of the charge already on the electrode (capacitor "plate") surfaces. The net result is then at a given voltage applied across the electrodes more charge can be stored on these capacitor plates in the presence of the protein than in its absence. In fact, the capacitance  $C$  is related to the charge  $Q$  stored on the plates (electrodes) and the potential difference  $U$  applied by  $C = Q/U$ . Thus, when oriented dipoles are present the capacitance of the system is increased.

If the frequency of the electrical field is high enough, the protein will not have time to reorient, since it takes time to overcome the viscous drag exerted by the solvent bath [33]. This means that as the frequency is increased one finds that the capacitance (and hence  $\epsilon'_r$ , see Eqn. 1) falls. The rotational relaxation time  $\tau$  for a (hard) sphere in a Newtonian fluid is

$$\tau = \xi / (2kT) \quad (12)$$

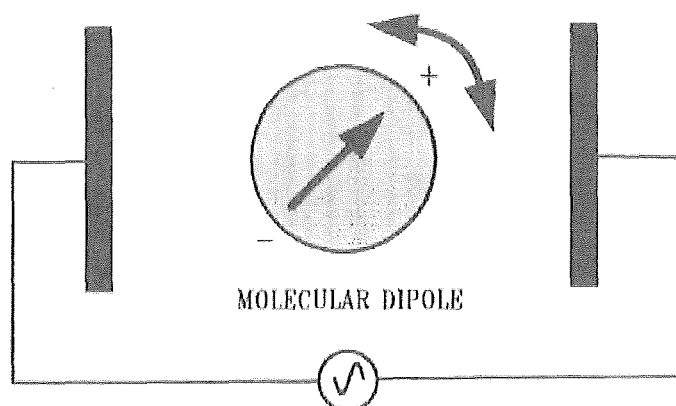


Fig. 9. The rotating dipolar billiard ball. In this model system of dielectric relaxation, the system of interest is a hard sphere possessing unit charges at opposite poles (i.e. it has a dipole moment). The alternating nature of the electric field means that the dipole seeks to rotate to an orientation of minimum energy with respect to the field.

where  $\xi$  is a molecular friction coefficient,  $k$  is Boltzmann's constant and  $T$  the absolute temperature.

If one models the protein as a hard sphere of radius  $a$ , rotating in a Newtonian fluid of viscosity  $\eta$ , the Stokes-Einstein relation gives  $\xi = 8\pi\eta a^3$ , so that

$$\tau = 4\pi\eta a^3 / (kT) \quad (13)$$

Thus one may expect (from Eqn. 4, and does indeed find) that the capacitance (or permittivity) of a protein solution is frequency-dependent, with the form of an inverted sigmoid when plotted against the logarithm of the frequency, and with the dispersion being half-completed, as usual, at a frequency  $f_c = 1/(2\pi\tau)$ .

The dielectric increment depends upon the molecular dipole moment  $\mu$ , the concentration of the protein, and other factors according to

$$\Delta\epsilon' = Ncg\mu^2 / (2\epsilon_0 MkT) \quad (14)$$

where  $N$  is Avogadro's number,  $c$  the protein concentration in  $\text{kg m}^{-3}$ ,  $g$  a parameter introduced by Kirkwood [35] to account for molecular associations,  $\mu$  the dipole moment in Debyes, and  $M$  the protein's molecular weight. Ellipsoidal globular proteins give dielectric spectra whose Cole-Cole  $\alpha$  is larger than 0; in the case of a very high axial ratio, separate relaxations of the two ellipsoids of revolution may be discerned [33]. Other processes, notably surface proton movements, which may contribute to the dielectric spectra of soluble proteins are discussed by Grant et al. [6], Pethig [8] and Takashima [17].

## 4. Mechanisms of dielectric relaxation in cell suspensions and tissues

### 4.1. Overview

A "classical" dielectric spectrum of a biological cell suspension or tissue (which may be treated as a concentrated suspension of cells) is illustrated in Fig. 10. This shows three major and two minor dispersions, which are usually attributed to: ( $\alpha$ ) the tangential flow of ions along cell surfaces, ( $\beta$ ) the build-up of charge at cell membranes via a Maxwell-Wagner effect, ( $\gamma$ ) rotation of small molecular weight dipoles, especially water, ( $\delta$ ) the rotation of macromolecular side-chains and "bound" water, and ( $\beta_1$ ) the rotation of intracellular proteins.

Not shown in Fig. 10, which is the "classical" representation, is a low-frequency  $\mu$ -dispersion [10, 36–38] observable in some membrane vesicle preparations and ascribed to various field-induced motions of membrane lipids and proteins. At all events, the take-home message is that *any* permanent or induced dipole may give rise to a dielectric dispersion.

Except for very-high-frequency work, which we cover but little here, electrodes are necessary to connect the measuring device to the sample of interest. This is because the current carriers in the wires are electrons whilst ions carry the current in the aqueous media characteristic of biological systems. The electrodes thus represent (and indeed are defined as) the interfaces between the measuring system and the measured system. As a result, what one measures in a system such as that of Fig. 1 is the behaviour of the electrodes *plus* the biosystem. At frequencies below 1 MHz or so the electrode effects (electrode polarisation) can often dominate the properties being measured. For reasons of space, this extremely important problem, and approaches to its solution, must

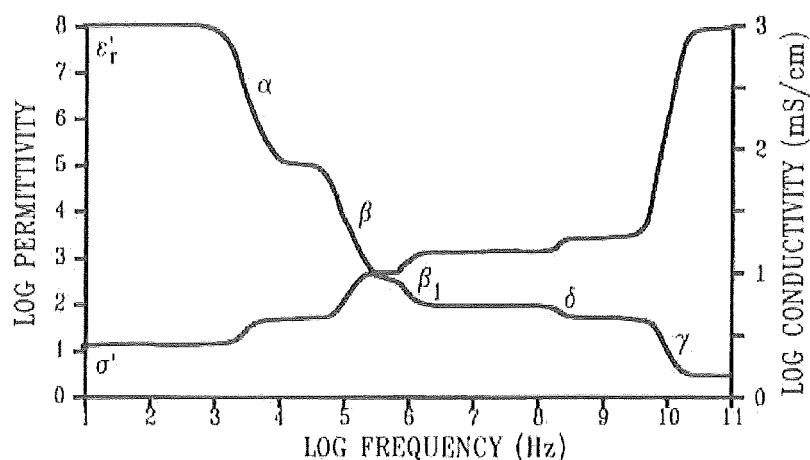


Fig. 10. Classical dielectric dispersions exhibited by a typical biological tissue.



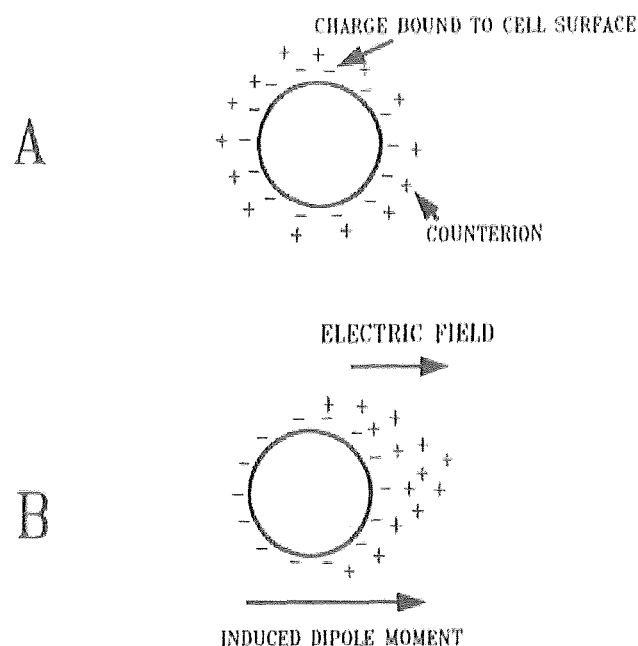


Fig. 11. (A) A cell with a net surface charge surrounded by a diffuse layer of counterions. (B) The production of an induced dipole moment by the application of an electric field.

remain largely outside the scope of the present chapter, but are discussed in many reviews (see, e.g., refs. 5, 6, 12, 39, 40, and references therein).

#### 4.2. The $\alpha$ -dispersion

Cell surfaces are generally negatively charged, but the surface charge density depends on the cell type [7, 41–43]. Thus, erythrocytes have neuraminic acid residues projecting from the glycoproteins and glycolipids of the plasma membrane forming part of their glycocalyx. Gram-positive bacteria have a high surface charge due to the teichoic acids in their cell walls, a feature of some taxonomic importance since Gram-negative bacteria lack these highly-charged wall components [44].

The presence of this cell surface charge results in a diffuse counterion layer around the cells as shown in Fig. 11A. When an electric field is applied to such a cell, the counterions move tangentially to the cell surface, resulting in the production of an induced dipole along the length of the cell (Fig. 11B). It is obvious that since the effective dipole moment is the product of the number of charges and the net distance moved, and the latter is the diameter of the cell, such induced dipole moments can be very large indeed. As it takes a finite time for the counterions on the cell surfaces to reach the end of the cells, one can see that the number of ions managing to do so will increase with decreasing frequency. This means (as usual) that the apparent relative permittivity

of the material between them drops as the frequency rises. As before, the permittivity falls and the conductivity rises between two plateau values as frequency is increased.

Several theoretical attempts to give a quantitative description of the  $\alpha$ -dispersion have been made, though none has been really successful because of the rather restrictive assumptions that underlie them [11]. Schwarz [45] has modelled the low-frequency dielectric properties of spherical colloidal particles which have a surface charge and found that the value of  $\tau$  is given by

$$\tau = Q_i r^2 / (2ukT) \quad (15)$$

where  $Q_i$  is the charge of the counterion,  $r$  is the radius of the particle (which must be much greater than the thickness of the electrical double layer around the particle) and  $u$  the surface mobility of the counterions. Given typical values of the parameters,  $f_c$  values for the  $\alpha$ -dispersion are expected to be around  $10^2$ – $10^3$  Hz. An important point to notice is that the value of  $\tau$  is proportional to the square of the radius. This is broadly consistent with the data observed, and is in contrast to the situation for the  $\beta$ -dispersion, where  $\tau$  is proportional to  $r$  (see later).

At frequencies well below the  $f_c$  of the  $\beta$ -dispersion (where the  $\alpha$ -dispersion is typically centred) the plasma membrane of biological cells effectively screens off the highly conducting cell interior. This means that to all intents and purposes the cell is a nonconductor suspended in a conducting suspending medium. If the cell is surrounded by a porous wall which contains fixed charges, then one would expect counterions to distribute themselves both inside and outside the wall [8]. A model for this system has been developed by Einolf and Carstensen [46] using an extension of the Schwarz model to account for the dielectric properties of suspensions of ion exchange resins [47]. They showed that the  $\tau$  value was successfully given by Eqn. 15. However, it may be noted that the Schwarz [45] model does not take into account a possible exchange of double layer counterions with the bulk phase.

Many studies have been undertaken to investigate the effects of the fixed surface charges on the low-frequency dielectric properties of bacterial suspensions [38, 48–55]. In all cases where a significant fixed surface charge was present the  $\epsilon'_c$  and  $\sigma'$  of the cells at low frequencies were too large to be accounted for by the  $\beta$ -dispersion alone. It thus appears that at low frequencies the cell surface charge and the resulting  $\alpha$ -dispersion make a very important contribution to the dielectric properties of bacterial cells.

Several investigations have been made on bacteria lacking cell walls, to see if one finds the expected reduction in the low-frequency  $\epsilon'_c$  and suspensions conductivity. Two studies have been done on the wall-less Mollicute group of bacteria. Carstensen et al. [53] showed that *Mycoplasma laidlawii* and *M. gallisepticum* both have small low-frequency

cell conductivities. However, Schwan and Morowitz's study [48] on an unidentified pleuropneumonia-like organism (PPLO) did demonstrate the presence of an  $\alpha$ -dispersion in the  $\epsilon'$  data, albeit one quite small compared to that of the  $\beta$ -dispersion. A substantial reduction or near total abolition of the  $\alpha$ -dispersion by removing the cell wall of bacteria (to produce protoplasts) has been seen in the studies of Einolf and Carstensen [52] and Harris and Kell [38]. In the latter study the magnitude of the residual  $\alpha$ -dispersion of the bacterial protoplasts could also be reduced by the addition of the cross-linking agent glutaraldehyde. This suggests that the  $\alpha$ -dispersion of bacteria must also contain contributions from the diffusional motions of proteins and/or lipids in the cell envelope.

As was stated earlier, one might expect that Gram-positive bacteria will in general have much larger  $\alpha$ -dispersions than Gram-negative bacteria by virtue of their more highly charged cell walls. Harris and Kell [38] studied one Gram-positive bacterial species (*Bacillus subtilis*) and two Gram-negative species (*Methylophilus methylotrophus* and *Paracoccus denitrificans*). Both *B. subtilis* and *P. denitrificans* had substantial  $\alpha$ -dispersions while *M. methylotrophus* did not. Although notionally Gram-negative, *P. denitrificans* is very sensitive to lysozyme in certain phases of growth (see, e.g., ref. 56). This serves to emphasize that more extensive and systematic studies of the correlation between wall structure and the  $\alpha$ -dispersion are needed. We also know of no data concerning the effect on the  $\alpha$ -dispersion of the presence or absence of charged capsules, or indeed of the effect of cell morphology generally.

The  $\alpha$ -dispersion of yeast (*Saccharomyces cerevisiae*) is notable by its absence [57–61], and this is also true for cultured animal cells [62–65]. However one cannot rule out the possibility of a small  $\alpha$ -dispersion being present, because the dielectric data at these very low frequencies in conductive media are inevitably distorted by electrode polarisation. Recent progress in eliminating such artefacts [40] may be expected to greatly improve our knowledge of the  $\alpha$ -dispersion.

The animal cell type that has been studied most extensively is the erythrocyte (red blood cell, R.B.C.). Schwan [66] has indicated that normal erythrocytes do not possess an  $\alpha$ -dispersion while erythrocyte ghosts do [67, 68]. (Ghosts are erythrocyte membranes prepared by osmotic treatment of erythrocytes, and lacking their normal internal contents.) The reason for this effect is not at all clear and it is likely that such things as the source (e.g. fresh as opposed to blood-bank blood) and the age and preparation of the blood will have some effect on the magnitude of the  $\alpha$ -dispersion seen. Ponder and Ponder [69] (see also ref. 70) showed that the electrophoretic mobility of erythrocyte ghosts varied with the preparation method and that the mobility of freshly washed erythrocytes decreased with storage time (at 4°C).

The major problem in working with whole blood is that it is highly conducting, so that electrode polarisation can become a severe problem at low frequencies. Figure 12 shows the  $\alpha$ -dispersion of erythrocytes

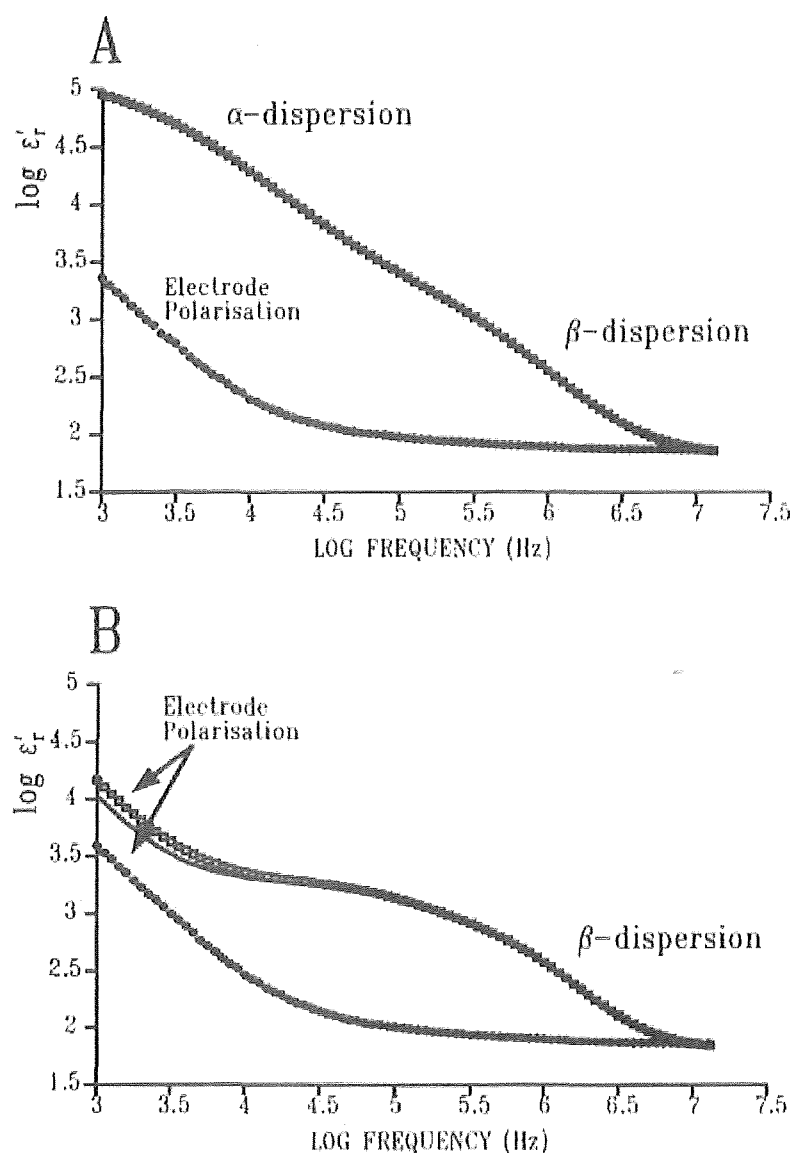


Fig. 12. The effect of neuraminidase treatment on the low frequency-dielectric properties of human erythrocytes. The blood was obtained from a hospital blood bank and was stored at 4°C until used. In order to reduce electrode polarisation the cells were washed three times and resuspended in a medium consisting of 1 mM NaCl, 0.5 mM KCl, 20 mM HEPES, 280 mM D-sorbitol, pH 7.60. After the first wash the cells were incubated at 37°C for 1 h to allow the pH to stabilise.  $2 \times 2$  ml aliquots of the stock blood suspension ( $3 \times 10^9$  cells  $\cdot$  ml $^{-1}$ ) were taken and one had 10 units of neuraminidase added. Both samples were then incubated at 37°C for 1 h before being washed once in phosphate buffered saline and then twice in the suspending medium. After this treatment the cells were again adjusted to  $3 \times 10^9$  cells  $\cdot$  ml $^{-1}$  in the suspending medium and their dielectric properties registered at 37°C as described by Davey et al. [40]. (A) The control (non-enzyme-treated) suspension and (B) the enzyme-treated suspension. The squares are the data actually measured, the diamonds are for a sample of the cell suspension medium adjusted to the same conductance (at 1 kHz) as the suspension, and the solid line represents permittivity data for all the cell suspension minus those for the adjusted medium (the principle behind this is explained in detail in ref. 40). The graphs clearly show the loss of the low frequency dispersion centred at about 10 kHz (the  $\alpha$ -dispersion) due to the removal of the neuraminic acid residues at the erythrocyte surface.

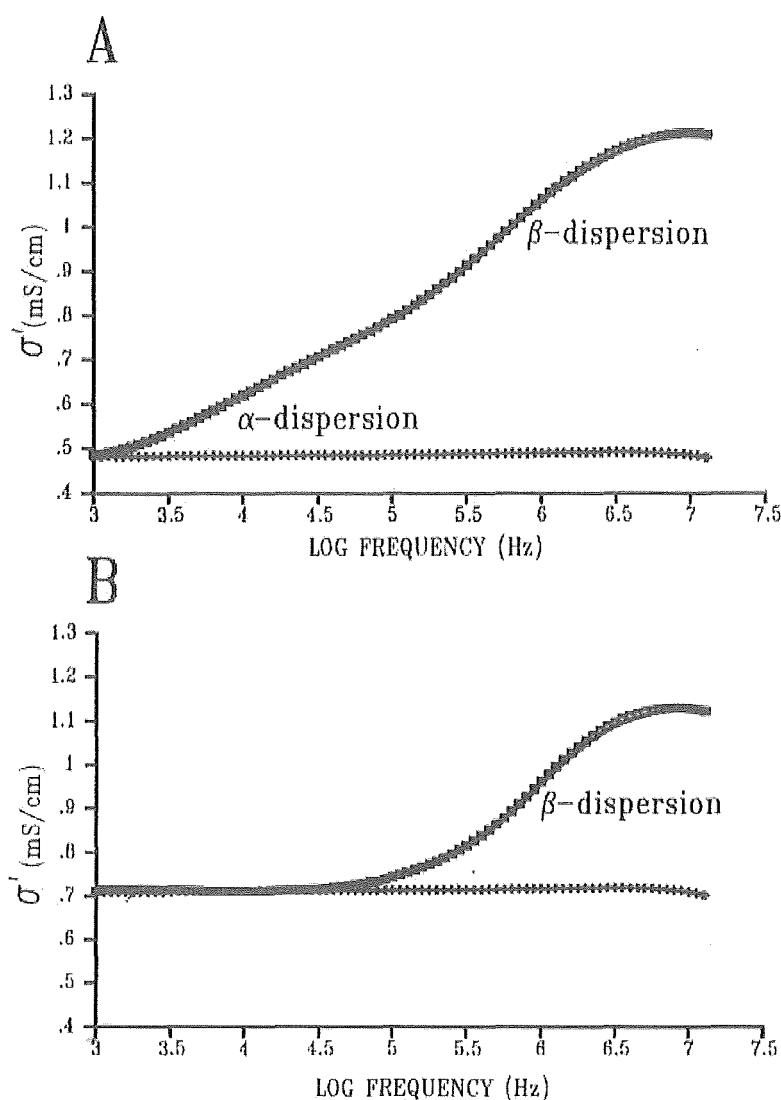


Fig. 13. The conductivity data equivalent to the permittivity data in Fig. 12. The symbols are the same as in Fig. 12 but for the conductivity data instead. Once again the loss of the  $\alpha$ -dispersion is clearly seen after the enzyme treatment.

that had been washed and resuspended in a sorbitol, low salts medium, and demonstrates that the surface charge of the R.B.C. that gives rise to the  $\alpha$ -dispersion is largely due to neuraminic acid residues. The cells in Fig. 12A were washed, and show substantial  $\alpha$ - and  $\beta$ -dispersions. Figure 12B shows cells of the same suspension after they had been treated with the enzyme neuraminidase. This enzyme removes the neuraminic acid residues from the cell surface and so reduces its surface charge. As one can see, the enzyme treatment has removed at least 90% of the  $\alpha$ -dispersion. Figure 13 displays the conductivity data equivalent to the permit-

tivity results shown in Fig. 12. Once again the loss of the  $\alpha$ -dispersion on the enzyme treatment is very clear.

It is not improbable that other factors may contribute to the  $\alpha$ -dispersion, as was alluded to above for bacteria. These processes may include such things as the field-induced gating of transmembrane ion transfers and it is certainly true to say that the classical explanations (see, e.g., refs. 71, 72) do not alone account for the independence of the magnitude of the  $\alpha$ -dispersion from the number and valency of counterions in bacterial chromatophores [36]. The  $\alpha$ -dispersion of muscle is known to be dominated by the access impedance of the sarcotubular system [11, 73, 74] but it probably still contains contributions from the normal  $\alpha$ -dispersion processes. Nonetheless, the low-frequency dielectric properties of extended, charged macromolecules such as DNA are clearly caused by counterion relaxation mechanisms of the type described earlier [75, 76]. Given the morphological and molecular complexity of biological cells, further theoretical and experimental developments in describing the  $\alpha$ -dispersion would benefit from the adoption of simpler experimental systems. Charged HPLC resins of uniform size and surface charge density seem an obvious candidate [77].

#### 4.3. The $\beta$ -dispersion

Biological membranes have conductances of the order of perhaps  $10^{-3} \text{ mS} \cdot \text{cm}^{-2}$  and may be regarded (with respect to the intracellular and extracellular spaces) as essentially nonconductors. On each side of this "insulator" are conducting ionic solutions (the cell cytoplasm and the suspending medium) and so a cell membrane is analogous to a classical electrical capacitor. This means that when an exciting potential difference is applied across a cell suspension the membrane capacitance  $C_m$  is charged up by ions moving under the influence of the electric field, i.e.,  $C_m$  is charged up via the conductivities of the cell medium,  $\sigma_o'$ , and the cytoplasm,  $\sigma_i'$ . Thus the membrane charging is equivalent to a resistor (reflecting  $\sigma_i'$  and  $\sigma_o'$ ) in series with a capacitor (reflecting  $C_m$  and the volume fraction  $P$  of cells). This series circuit is then in parallel with a resistor equivalent to the current flowing around the cells and a capacitor reflecting the high-frequency residual permittivity of the suspension. Like all such networks it possesses a time constant (relaxation time; equivalent to  $RC$ ), which reflects the time taken to charge up the membranes. An equivalent circuit for this arrangement is given in Fig. 14, together with the highly oversimplified structure of a cell in the suspension which this model assumes.

The physical interpretation of this electrical model is that as the frequency  $f$  rises, fewer and fewer ions have time to charge up the membrane(s) before the field changes direction. Thus the charge stored

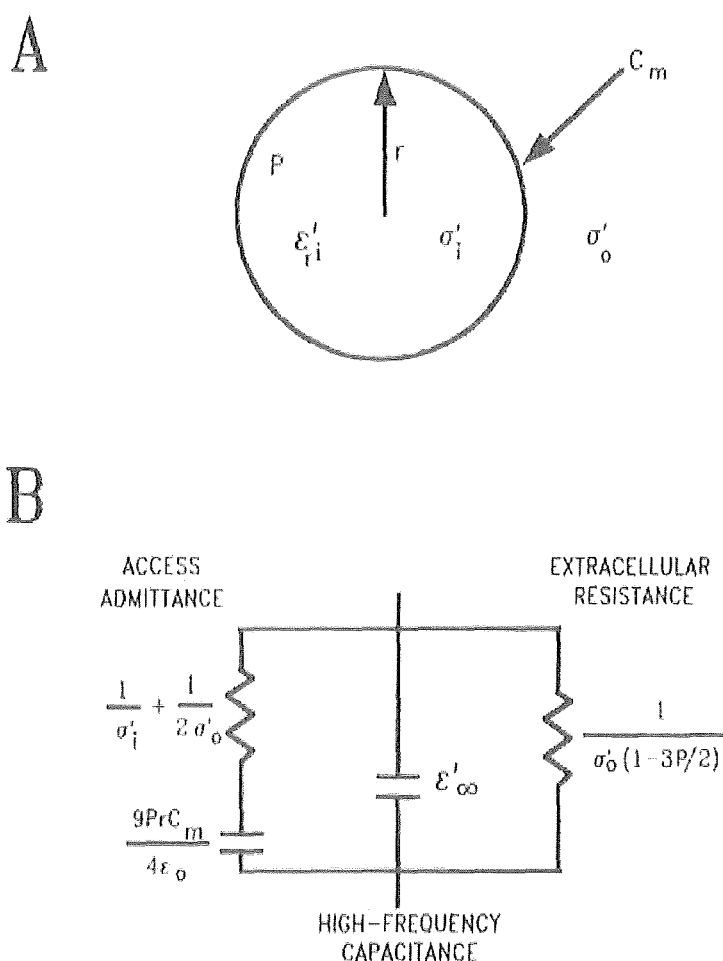


Fig. 14. A model used to characterise the dielectric properties of cell suspensions, (A) A spherical cell of radius  $r$ , membrane capacitance per unit area  $C_m$ , and internal and external conductivities of  $\sigma'_i$  and  $\sigma'_o$ , respectively. The internal permittivity of the cell is  $\epsilon'_{ti}$ . (B) The equivalent circuit of a suspension of such cells present at a volume fraction  $P$ , together with the equivalent physical parts of the system to which they refer.

by the suspension for a given exciting potential difference falls and the capacitance and permittivity of the suspension drops with increasing frequency. At low frequencies the admittance (conductance to alternating current) of the cell membranes is very low and so the cells behave as non-conductors suspended in a conducting medium. This means that most of the current must flow around the cells. As the frequency increases, the membrane's admittance rises and an increasing amount of current can flow through the membranes and the relatively highly conducting cytoplasm of the cells; thus the conductivity of the suspension increases. This fall in permittivity and rise in conductivity with increasing frequency is illustrated in Fig. 15.

Although the dominant processes underlying the  $\beta$ -dispersion can be seen purely in terms of the above equivalent circuit, it should not be

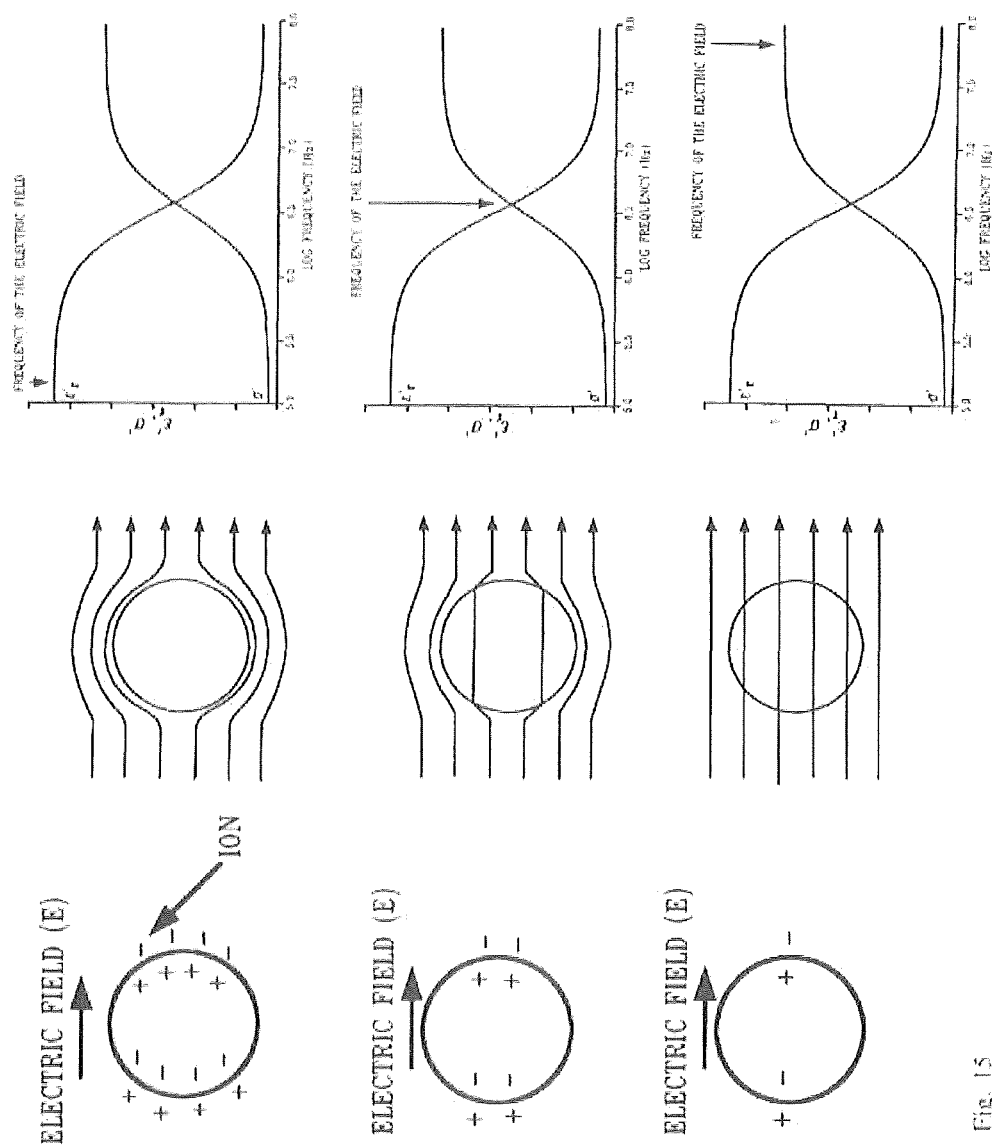


Fig. 15



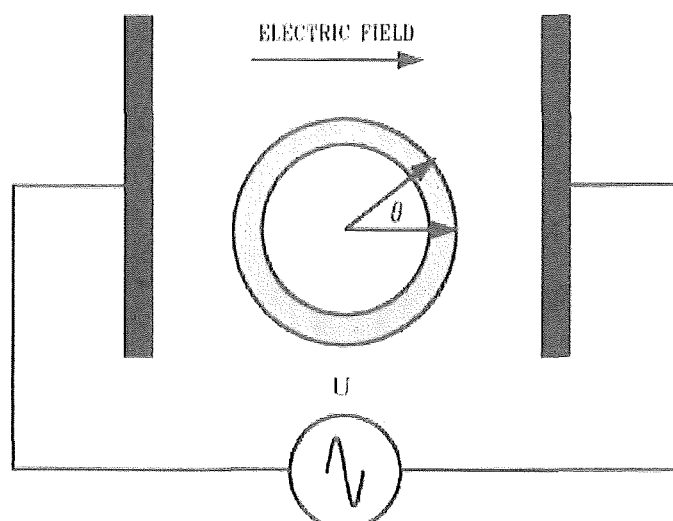


Fig. 16. The amplification by the plasma membrane of an applied exogenous electric field. For a full discussion see text. The angle  $\theta$  on the diagram allows one to calculate the field-induced membrane potential at any point on the plasma membrane when used in conjunction with Eqn. 16.

forgotten that the underlying physical process is a Maxwell-Wagner interfacial type of polarisation due to the differences in complex permittivities between the cells and the medium. Also, one should not forget that the basic idea underlying dielectric theory generally is the presence in the sample of permanent or induced dipoles. Very few references on the  $\beta$ -dispersion, as observed at low field strengths, deal with the idea that one can regard the  $\beta$ -dispersion as producing a dipole across the cell (but see ref. 78). However, the effect of the processes which can be observed as the  $\beta$ -dispersion in causing such high-electric-field phenomena as cell rotation is often expressed in terms of dipoles [79].

As the admittance of the cell plasma membrane increases, and the extent to which it is charged decreases with increasing frequency during the  $\beta$ -dispersion, one can see that the potential difference induced across the membrane must also decrease. The induced membrane potential  $\Delta\phi_m$ , which adds vectorially to any naturally occurring one, is given by

$$\Delta\phi_m = 1.5rE_0 \cos \theta / [1 + (f/f_c)^2]^{1/2} \quad (16)$$

where  $r$  is the cell radius,  $E_0$  is the applied exogenous field strength,  $\theta$  is the angle shown in Fig. 16 and  $f$  and  $f_c$  are, respectively, the frequency of the applied field and the critical frequency of the  $\beta$ -dispersion. This

Fig. 15. The effect of frequency upon the polarisation, current flow and dielectric properties of spherical shell suspensions. The frequency increases from top to bottom. It is assumed that the electrodes are to the right and left of the cells illustrated, and that the system observed at an instant when the right-hand electrode is negative. The left-hand portion shows the relative polarisation of the plasma-membrane, the middle portion the flow of current around and/or through the cells, and the right-hand portion the approximate frequency (relative to  $f_c$ ) at which the behaviour indicated would be observed. For further discussion see text.

induced membrane potential  $\Delta\phi_m$  then drops across the very thin plasma membrane, resulting in a very considerable induced field across the membrane (see, e.g., refs. 79–81). This field amplification effect has two major consequences. The first is that the proteins in the membrane can easily be exposed to quite high local field strengths in low-level exogenous fields, resulting in the reorganisation of their dipolar structures and hence to effects on their biological properties. The consequences of this are considered later in the context of nonlinear effects. The second consequence is that when high exogenous field strengths are applied to the cells the very high induced fields can result in the breakdown of the membrane. This phenomenon, and such processes as gene transfer and cell fusion which may follow from it, are now of great importance in biotechnology.

The fall in  $\epsilon'_i$  and rise in  $\sigma'_i$  of the  $\beta$ -dispersion may be modelled by the appropriate Debye equations (Eqns. 4 and 11). The values of  $\Delta\epsilon'_i$ ,  $\Delta\sigma'_i$  and  $\tau$  to be inserted into the equations can be calculated from Schwan's equations for the  $\beta$ -dispersion of a suspension of spherical cells [26]:

$$\Delta\epsilon'_i = 9PrC_m/(4\epsilon_o) \quad (17)$$

$$\sigma'_i = \sigma'_o(1 - 3P/2) \quad (18)$$

$$\sigma'_h = \sigma'_o[1 + 3P(\sigma'_i + \sigma'_o)/(\sigma'_i + 2\sigma'_o)] \quad (19)$$

$$\tau = rC_m[1/\sigma'_i + 1/(2\sigma'_o)] \quad (20)$$

where the symbols used are those described in Figs. 4 and 14.

Over the years, many sets of equations have been derived to describe the  $\beta$ -dispersion of cells. Single-shell models describing cells or vesicles with a plasma membrane and homogeneous cell contents and suspending media have been given by (among many others) Fricke [82] and Schwan [26]. Modified models of cells have been made to allow for the presence of internal membrane-bound organelles [62, 83] and the presence of a wall external to the plasma membrane [58, 60, 84]. Theoretical expressions have also been derived for nonspherical cells [82, 84–88].

Equation 17 shows that the  $\Delta\epsilon'_i$  value of the  $\beta$ -dispersion one expects for a given volume fraction is proportional both to the cells' membrane capacitance per unit area,  $C_m$ , and the (mean) cell radius,  $r$ . As the value of  $C_m$  appears to be approximately  $1 \pm 0.5 \mu\text{F}/\text{cm}^2$  for biological cells [89], then one would expect the literature values of  $\Delta\epsilon'_i/P$  to increase linearly with cell radius. However care has to be taken when extracting the  $\Delta\epsilon'_i/P$  values from the literature as one must ensure that the volume fractions used are less than 0.2 to 0.3 because above this  $\Delta\epsilon'_i/P$  ratio is no longer constant [11, 61]. At volume fractions greater than 0.2 to 0.3 electrical interactions between the cells start to occur and this results in the  $\Delta\epsilon'_i$  for a given  $P$  being less than that expected from Eqn. 17. This

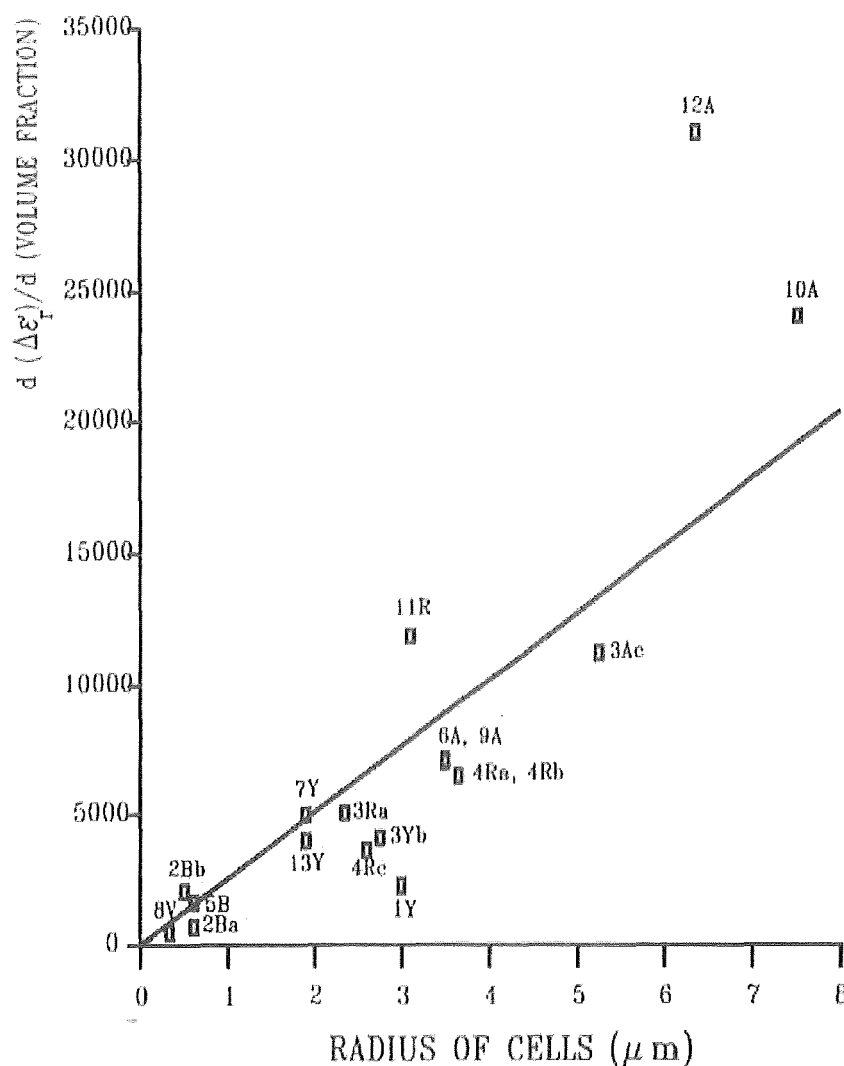


Fig. 17. Some literature values for  $d(\Delta\epsilon')/dP$  extracted from the linear low volume fraction portions of  $\Delta\epsilon'$  versus volume fraction ( $P$ ) graphs. The upper case letters next to the data points refer to the type of cell measured. V = vesicle, B = bacteria, Y = yeast, R = red blood cells and A = animal cells (other than red blood cells). The numbers refer to the reference used to extract the data plotted. The solid line is for a membrane capacitance of  $1 \mu\text{F}/\text{cm}^2$ . 1: ref. 57, *Saccharomyces cerevisiae*, 17°C; 2: ref. 116, a = *Halobacterium halobium*, b = *Halobacterium marismortui*, both at 25°C; 3: ref. 87, a = spherical rabbit R.B.C., b = *Saccharomyces cerevisiae*, c = rabbit leucocytes, all at 21°C; 4: ref. 192, a = dog R.B.C., b = rabbit R.B.C., c = sheep R.B.C., all at 21°C; 5: ref. 84, *Escherichia coli*; 6: ref. 193, mouse lymphocytes, 20°C; 7: ref. 58, *Saccharomyces cerevisiae*, 14°C; 8: ref. 108, rat brain cortex synaptosomes, 25°C; 9: ref. 194, mouse lymphocytes, 20°C; 10: ref. 64, cultured rat basophil leukaemia cells, 30°C; 11: ref. 88, human R.B.C.; 12: ref. 65, LS-L929 mouse fibroblasts, 37°C; 13: ref. 61, *Saccharomyces cerevisiae*, 20°C.

fact has not been taken into account by many authors, particularly those working with tissues, who have calculated values of  $C_m$  (and so forth) from data at volume fractions where the equations do not apply (thus underestimating  $C_m$ ). Modifications to the standard equations to

allow for these non-linear effects at high volume fractions have proved problematic [11] but attempts have been made [11, 90a]. To prevent any errors due to these effects, the  $\Delta\epsilon'_r/P$  data for the  $\Delta\epsilon'_r/P$  versus  $r$  graph shown in Fig. 17 were taken from the gradient of  $\Delta\epsilon'_r$  versus  $P$  graphs in the linear "low  $P$ " region. As can be seen from Fig. 17 the relationship between  $\Delta\epsilon'_r/P$  and cell radius  $r$  is in good agreement with that expected for the  $\beta$ -dispersion. The scatter in the data may be taken largely to reflect differences in  $C_m$  between cell types.

Equation 17 also shows that the dielectric increment  $\Delta\epsilon'_r$  of the  $\beta$ -dispersion is proportional to the volume fraction of cells,  $P$ . Thus, if one monitors the permittivity (capacitance) of a cell suspension at a fixed frequency in the low-frequency plateau region then the signal measured will be proportional to the volume fraction of cells present (provided  $rC_m$  is approximately constant and that the  $P$  value does not exceed 0.2 to 0.3). As the measurement of biomass is of critical importance in fermentation technology [91, 92], this laboratory has developed a dielectric spectrometer (the Biomass Monitor, formerly called the  $\beta$ ugmeter) suitable for monitoring the biomass of fermentation broths and based on the above principles (see, e.g., refs. 92-98a).

Figure 18 shows some literature values for the membrane capacitance  $C_m$  of various cell types. As may be seen from the graph the majority of the  $C_m$  values are clustered about the expected  $1 \mu\text{F}/\text{cm}^2$  value that is often taken as a "constant" for all biological cells. The cell types that show the greatest variations in  $C_m$  are animal cells. The extremely large values of membrane capacitance all from ref. 99, which uses transmembrane electrodes) are for muscle cells. This effect has frequently been seen in the past and indeed led to the discovery of the sarcotubular system of muscle [73]. At low frequencies the sarcotubular system becomes charged up on the application of an electric field and this results in an increase in the permittivity of the cells. Thus, the measured permittivity is not due solely to the charging up of the plasma membrane but contains a substantial component from the sarcotubules. This in turn leads to an apparently artificially high value of  $C_m$  when it is calculated from the measured permittivities [11].

The high values for the membrane capacitance from the animal cell suspensions given by Surowiec et al. [63] and Davey et al. [65] on the diagram demonstrate the effect of cell surface morphology on the membrane capacitance. In both these cases the cells had highly folded plasma membranes which resulted in the true membrane area being very large in comparison to the area estimated by measuring the cells' diameter and assuming them to be spherical. As the membrane area was so high it gave the cells an abnormally large  $\Delta\epsilon'_r/P$  value for their visually observable radius. Thus, when  $C_m$  was estimated using the measured cell radii  $r$ , the resulting values were much higher than expected. Similar effects of surface morphology on  $C_m$  have been reported by Rothschild [100], and by Irimajiri et al. [101].

The fact that most of the  $C_m$  values in the literature are clustered about  $1 \mu\text{F}/\text{cm}^2$  is in itself problematic. Black lipid membrane studies have shown that the capacitance one would expect for a lipid bilayer is about half that measured for biological membranes (see ref. 55 and many references therein). In the classical explanation of the  $\beta$ -dispersion,  $C_m$  is a static membrane capacitance. However, studies of the effect of cross-linking agents [37, 38] and temperature [55] on the  $\beta$ -dispersion of natural membranes imply that the discrepancy may be due in part to the partially restricted motion of charged membrane lipids and proteins in such membranes.

Figure 19 is a plot of some literature values for the internal conductivity  $\sigma'_i$  of cells. It is clear that the greatest spread of  $\sigma'_i$  values occurs amongst the bacteria. The two very high internal conductivities are for the archaebacteria *Halobacterium halobium* ( $\sigma'_i = 40 \text{ mS}/\text{cm}$ ) and *H. marismortui* ( $\sigma'_i = 58 \text{ mS} \cdot \text{cm}^{-1}$ ). As both these bacteria are halophiles the very high  $\sigma'_i$  values are in line with expectations. The other clear trend in the bacterial data is that the Gram-positive organisms generally have higher internal conductivities than the Gram-negatives. Again, this has a known physiological basis, since Gram-positive bacteria generally have higher  $\text{K}^+$  contents than do Gram-negative ones [102].

The only other clear feature shown in Fig. 19 is the fact that both erythrocytes and other animal cells have internal conductivities of about  $5 \text{ mS}/\text{cm}$ . Pauly and Schwan [103] determined the electrical conductivity of the erythrocyte cytoplasm at frequencies of between 70 and 100 MHz. At these frequencies the membrane capacitance of the cells is completely shorted out, and the cells behave as conductive particles embedded in a conductive suspending medium. These authors found that the  $\sigma'_i$  values for erythrocytes of different species were all approximately  $5 \text{ mS}/\text{cm}$ . They also showed that after the haemoglobin content of the cells had been taken into account the internal conductivity of the cells was roughly half the expected value. This implied that the ions in the cells had a lower than expected mobility, either due to hydrodynamic or electrostatic effects. What is also clear from this work is that the  $\sigma'_i$  values calculated from high frequency spot readings agree well with those derived using data from the  $\beta$ -dispersion at lower frequencies.

Figure 20 shows a literature survey of the internal permittivities  $\epsilon'_n$  of cells. The reason for the rather wide range of permittivity values for bacteria is not clear (the halobacterial values exceeding 400 are probably contaminated by electrode polarisation artefacts), but on the whole most cells have values of  $\epsilon'_n$  of some 50 to 60. This is in line with the permittivity at these frequencies of water in the cytoplasm being reduced by the presence of ions and by the volume fraction of proteins present [13]. Most proteins would not be rotated by the field at the (high) frequencies at which the  $\beta$ -dispersion is complete and so would give a net permittivity decrement [6]. Once again the values of  $\epsilon'_n$  derived from the  $\beta$ -dis-

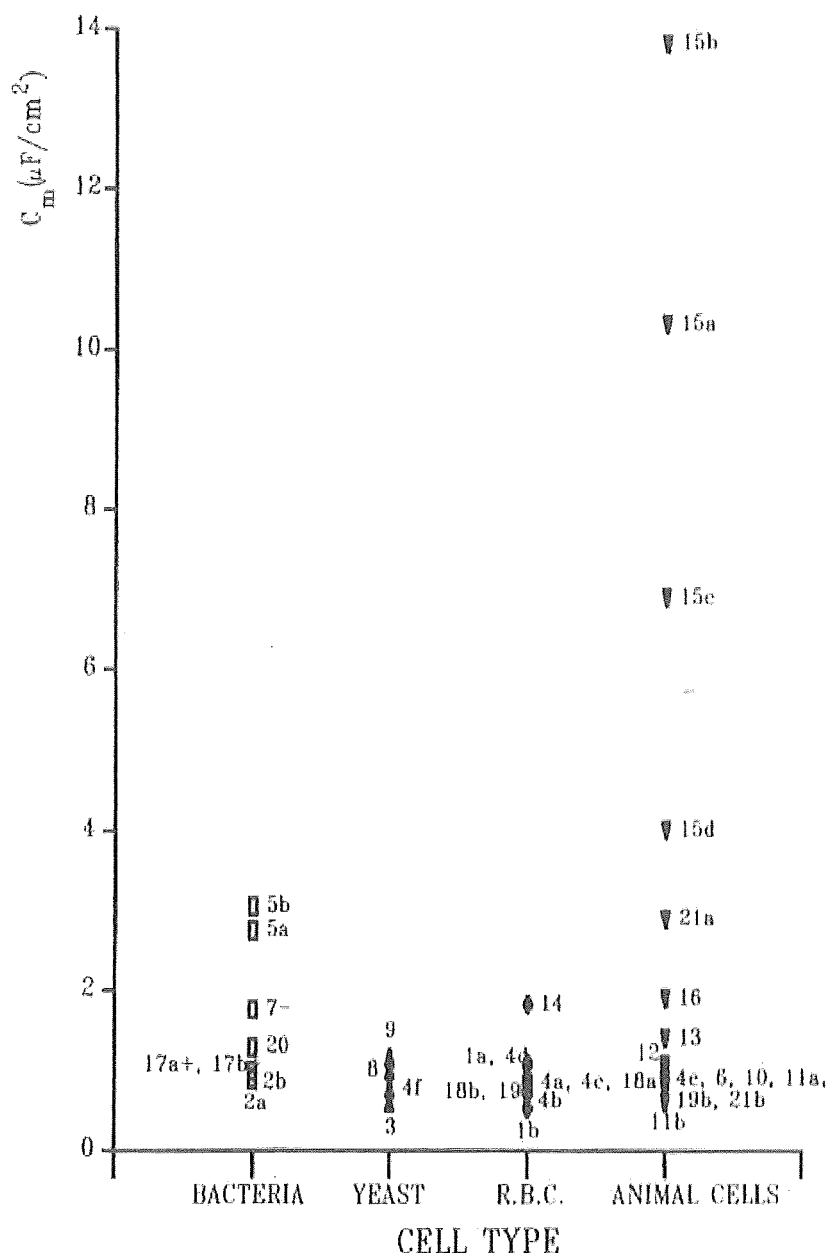


Fig. 18. A plot of some literature values of  $C_m$  versus their cell types. The "+" and "-" symbols for the bacteria are for Gram-positive and Gram-negative organisms, respectively. The numbers refer to the source of the data. 1: ref. 195, a = normal human R.B.C., b = human homozygous  $\beta$ -thalassaemic R.B.C., both at 25°C; 2: ref. 53, a = *Mycoplasma laidlawii*, b = *Mycoplasma gallisepticum*; 3: ref. 196; 4: ref. 192, a = dog R.B.C., b = rabbit R.B.C., c = sheep R.B.C., d = spherical rabbit R.B.C., e = rabbit leucocytes, f = *Saccharomyces cerevisiae*, all at 21°C; 5: ref. 116, a = *Halobacterium halobium*, b = *Halobacterium marismortui*, both at 25°C; 6: ref. 62, mouse lymphoblasts, 25°C; 7: ref. 84, *Escherichia coli*; 8: ref. 57, *Saccharomyces cerevisiae*, 17°C; 9: ref. 58, *S. cerevisiae*, 14°C; 10: ref. 193, mouse lymphocytes, 20°C; 11: ref. 197 a = squid axon membrane at 1 kHz, b = same as "a" at 50 kHz, both at 20°C; 12: ref. 194, mouse lymphocytes, 20°C; 13: ref. 64, cultured rat basophil leukaemia cells, 30°C; 14: ref. 88, human R.B.C.; 15: ref. 99, a = *Anolis cristatellus* white iliofibularis muscle (IFM), b = *Sceloporus occidentalis* white IFM, c = *Dipsosaurus dorsalis* white IFM, d = same as "c" but red IFM, all at 25°C; 16: ref. 65, LS-L929 mouse fibroblasts, 37°C; 17: ref. 98, a = *Micrococcus lysodeikticus* intact cells, b = same as "a" except are protoplasts; 18: ref. 198, a = human R.B.C. at 1 kHz, b = same as "a"

persion and from high-frequency measurements agree well with each other.

Like most low-frequency biological dispersions the  $\beta$ -dispersion of a cell suspension appears to have a distribution of relaxation times. This results in the dielectric spectrum measured having a Cole-Cole  $\alpha$  value greater than zero and, as one would expect from the earlier discussions, the  $f_{c,\alpha}$  is always higher than the  $f_{c,\beta}$ . Figure 21 shows the Cole-Cole  $\alpha$  values for different cell types as extracted from the literature. The most obvious feature of the plot is the extremely wide variation in the values for  $\alpha$  of *bacterial* cells. The  $\alpha$  values of 0.1 and zero are from Pauly [78] (number 13 on the diagram), the upper value being for intact cells of *Micrococcus lysodeikticus*, while the lower value is for protoplasts of the same bacterium. This fall in  $\alpha$  on removal of the bacterial cell wall was also observed by Harris and Kell [38], who interpreted it to indicate that the spherical protoplasts were electrically more isotropic and homogeneous than intact cells.

There is also a wide spread in the values of the Cole-Cole  $\alpha$  reported for yeast cells; in this case there is strong evidence that the  $\alpha$  value is markedly dependent on the growth phase of the cells. Markx et al. [96] measured the Cole-Cole  $\alpha$  of a strain of *Saccharomyces cerevisiae* during the course of a fermentation, and showed that the  $\alpha$  value changed from about 0.33 in the growth phase to 0.2 in the stationary one. From Eqn. 20 one could argue that this effect was due to variations in cell size over the course of the fermentation. However, flow cytometric measurements of the cell size distributions [104–107] were carried out, which showed that these did not provide a spread of relaxation times that could account for the high Cole-Cole  $\alpha$  values observed (see also ref. 10). Also no correlation between the variations in  $\alpha$  and cell size distribution was seen. Finally, realistic variations in internal conductivity could not account for the magnitudes of  $\alpha$  [96].

This failure of cell size distributions to explain the size of the Cole-Cole  $\alpha$  of a cell suspension has frequently been seen before (see, e.g., refs. 10, 64, 84, 108, 109). As the yeast used in the study of Markx et al. [96] was almost spherical, one can rule out the effect of cell shape in this case. It is worth pointing out that *significant* changes in shape towards bacillary [38, 78] or invaginated morphologies [64, 65, 101] *are* certainly accompanied by increases in the Cole-Cole  $\alpha$ . As distributions in cell size fail to explain the  $\alpha$  values seen, various authors have attempted to account for it using distributions in  $\sigma'_i$  [101, 108]. None of these attempts has been wholly successful and, indeed, Markx et al. [96] showed that major

---

except at 10 kHz; 19: ref. 199, a = spherical mouse R.B.C., b = mouse lymphocytes, both at 24°C; 20: ref. 48, PPLQ; 21: ref. 63, a = human B lymphocytes, b = human T lymphocytes, both at 24°C.

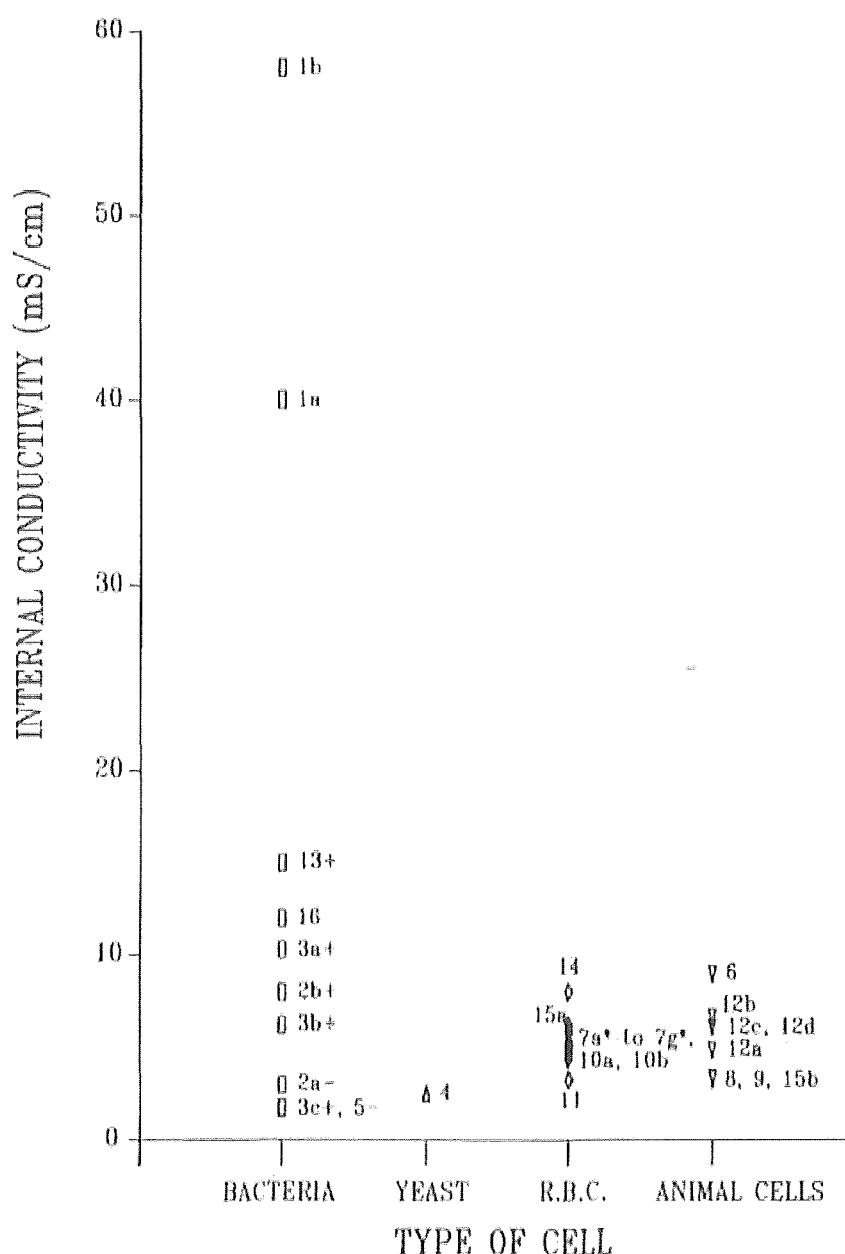


Fig. 19. Literature values for the internal conductivity of cells. The "+" and "-" symbols on the bacteria data refer to the cells Gram stain and the "\*" symbol on the blood data refer to values calculated from high-frequency methods. The numbers refer to the data source. 1: ref. 116, a = *Halobacterium halobium*, b = *Halobacterium marismortui*, both at 25 °C; 2: ref. 50, a = *Escherichia coli*, b = *Micrococcus* sp., both at 25 °C; 3: ref. 54, a = *Streptococcus faecalis*, b = *Micrococcus* sp., c = *Micrococcus lysodeikticus*; 4: ref. 58, *Saccharomyces cerevisiae*, 14 °C; 5: ref. 84, *E. coli*; 6: ref. 193, mouse lymphocytes, 20 °C; 7: ref. 200, a = human R.B.C., b = beef R.B.C., c = sheep R.B.C., d = dog R.B.C., e = cat R.B.C., f = rabbit R.B.C., g = chicken R.B.C., all at 25 °C; 8: ref. 194, mouse lymphocytes, 20 °C; 9: ref. 64, cultured rat basophil leukaemia cells, 30 °C; 10: ref. 195, a = normal human R.B.C., b = human homozygous  $\beta$ -thalassaemic R.B.C., both at 25 °C; 11: ref. 88, human R.B.C.; 12: ref. 99, a = *Anolis cristatellus* white iliofibularis muscle (IFM), b = *Sceloporus occidentalis* white IFM, c = *Dipsosaurus dorsalis* white IFM, d = same as "c" but red IFM, all at 25 °C; 13: ref. 78, *Micrococcus lysodeikticus*; 14: ref. 201, *Cyprinus carpio* R.B.C., 25 °C; 15: ref. 199, a = spherical mouse erythrocytes, b = mouse lymphocytes, both at 24 °C; 16: ref. 48, PPLO.



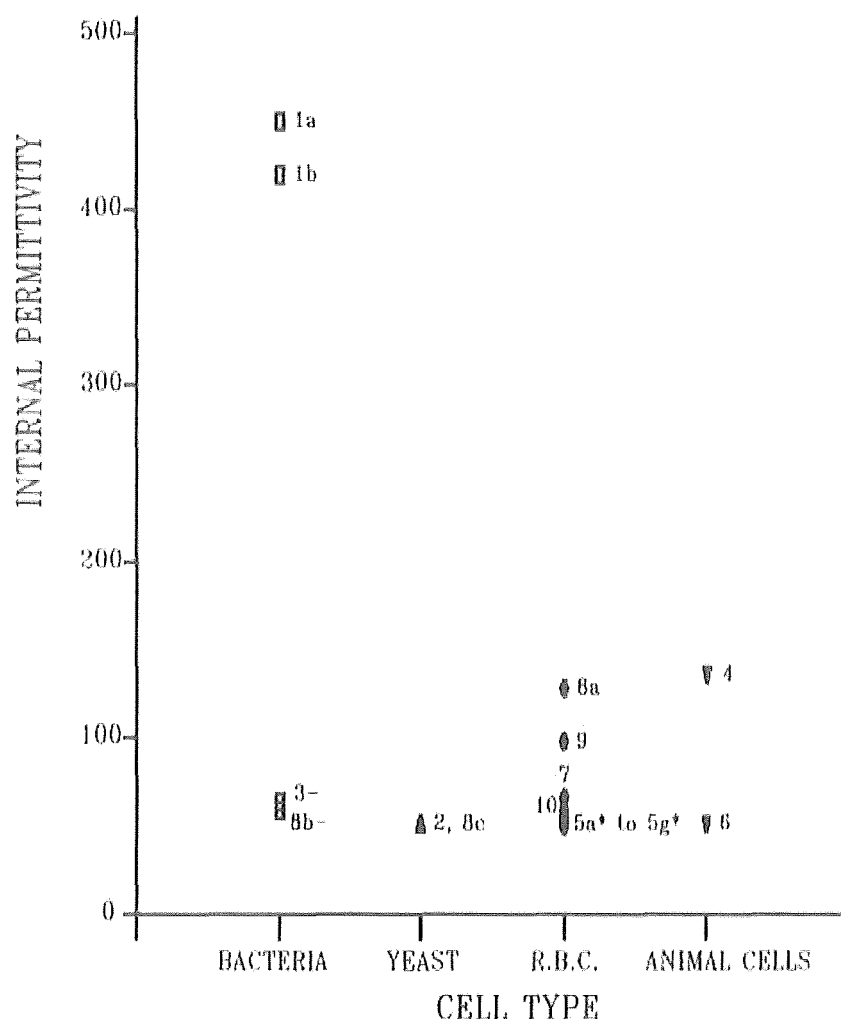


Fig. 20 Internal permittivities as extracted from the literature. The "+" and "-" symbols refer to the bacterial Gram stain, while asterisks indicate high frequency results. The numbers refer to the source reference. 1: ref. 116, a = *Halobacterium halobium*, b = *Halobacterium marismortui*, both at 25°C; 2: ref. 58, *Saccharomyces cerevisiae*, 14°C; 3: ref. 84 *Escherichia coli*; 4: ref. 195, mouse lymphocytes, 20°C; 5: ref. 200, a = human R.B.C., b = beef R.B.C., c = sheep R.B.C., d = dog R.B.C., e = cat R.B.C., f = rabbit R.B.C., g = chicken R.B.C., all at 25°C; 6: ref. 194, mouse lymphocytes, 20°C; 7: ref. 88, human R.B.C.; 8: ref. 202, a = human R.B.C. at 25°C, b = *E. coli* at 26°C; 9: ref. 201, *Cyprinus carpio*, 25°C; 10: ref. 199, spherical mouse erythrocytes, 24°C.

distributions in the values of  $C_m$ ,  $\sigma'_i$  and cell size, and various combinations of these, failed to explain the  $\alpha$  values of their yeast cell suspensions.

Since variations in any of the parameters underlying the classical explanation of the  $\beta$ -dispersion are not nearly large enough to account for the large values of the Cole-Cole  $\alpha$  seen (or, one might better say, fitted to the data), one is led to the conclusion that other dispersive mechanisms must be contributing to the classical  $\beta$ -dispersion. The cause

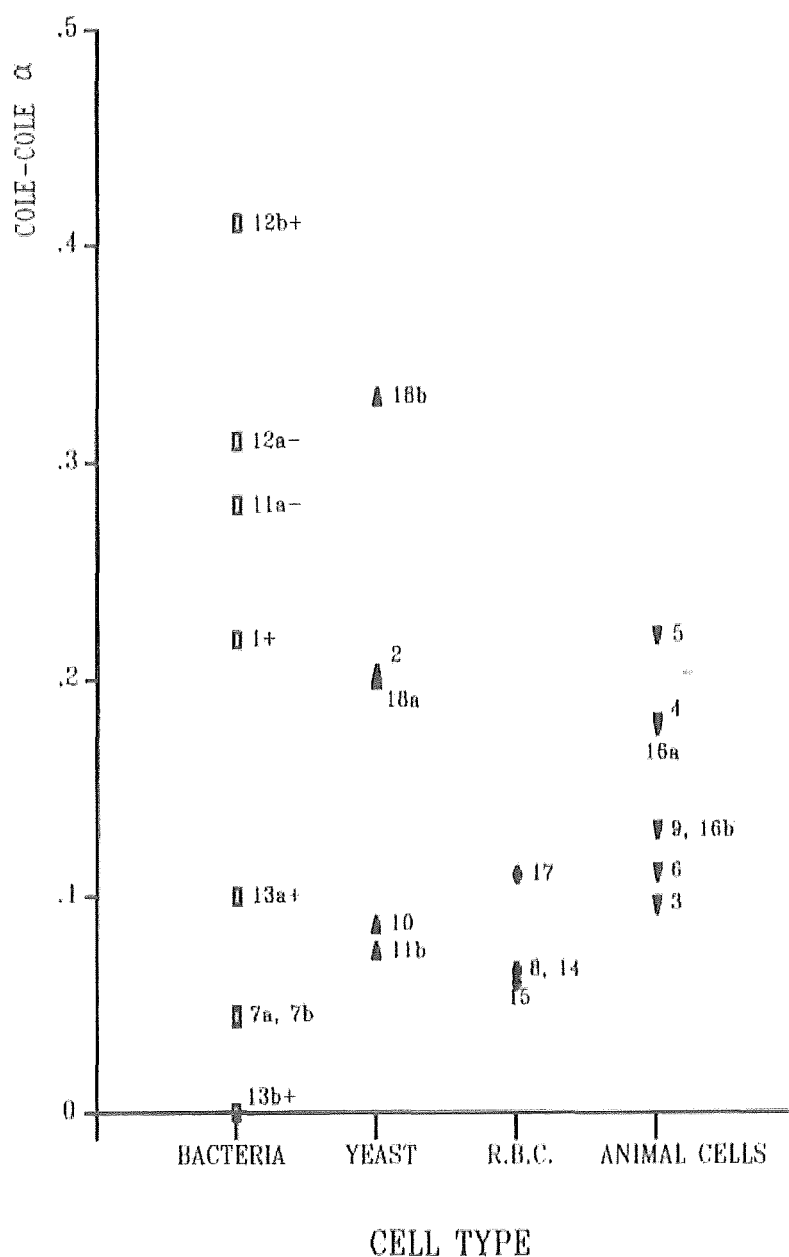


Fig. 21. Literature values of the Cole-Cole  $\alpha$ . The "+" and "-" signs refer to the Gram stain of the bacteria whilst the numbers refer to the source material. 1: ref. 203, *Staphylococcus aureus*, 27°C; 2: ref. 58 *Saccharomyces cerevisiae*, 14°C; 3: ref. 62, cultured mouse lymphoblasts, 25°C; 4: ref. 193, mouse lymphocytes, 20°C; 5: ref. 195, mouse lymphocytes, 20°C; 6: ref. 64, rat basophil leukaemia cells, 30°C; 7: ref. 116, a = *Halobacterium halobium*, b = *Halobacterium marismortui*, both at 25°C; 8: ref. 15, human R.B.C., 37°C; 9: ref. 65, LS-L929 mouse fibroblasts, 37°C; 10: ref. 61, *S. cerevisiae*, 20°C; 11: ref. 55, a = *S. cerevisiae* at 30°C, b = *Escherichia coli* at 25°C; 12: ref. 38, a = *Methylophilus methylotrophus* at 37°C, b = *Bacillus subtilis* at 25°C; 13: ref. 78, a = intact cells of *Micrococcus lysodeikticus*, b = as in "a" except are protoplasts; 14: ref. 202, human R.B.C., 18°C; 15: ref. 201, *Cyprinus carpio*, 22°C; 16: ref. 63, a = human T lymphocytes, b = human B lymphocytes, both at 24°C; 17: ref. 18, human R.B.C., 37°C; 18: ref. 96, *S. cerevisiae*.

of these contributions most probably involves the lateral mobility of membranous components [10, 13, 15, 36–38]. This idea has the merits of explaining (for the  $\beta$ -dispersion) each of the following sets of observations, which have been widely recorded and which are not consistent with the simple, classical picture; (i) the positive temperature coefficient observed for the dielectric increment, (ii) the fact that the value of  $C_m$  calculated for *biological* membranes is significantly greater than that observed for pure (and solvent-free) lipid membranes, (iii) the sensitivity of the  $\beta$ -dispersion to chemical cross-linking agents, and (iv) the excessive magnitude of the Cole-Cole  $\alpha$  typically observed.

#### 4.4. Membrane properties and the $\beta$ -dispersion

The electronic biomass probe that has been derived in this laboratory for the registration of the biomass in fermentors has been alluded to above. It is important to note that the dielectric increment of the  $\beta$ -dispersion correlates with *viable* biomass, and not simply with cell number [110, 111, 111a]. This is because dead cells do not have intact membranes and so do not contribute to the  $\beta$ -dispersion measured. This has been confirmed by many studies on the fundamental processes underlying the  $\beta$ -dispersion that have involved treating cells with membrane-lytic agents [60, 110–116]. Indeed, the fact that one can use the charging up of membranes as a sensitive means of detecting drug and other chemical interactions with membranes has also been exploited. Whole cell studies include those of Asami et al. [60], Lap et al. [117], Pliquett and Wunderlich [118] and Stoicheva et al. [111]. Studies on black lipid membranes enable one to gain information on the effects of the drug or chemical on the substructure of the membrane, and studies exploiting this include the work of Coster et al. [119] and Perez and Wolfe [120].

Given that, as has been known for many years [26, 121–123], the dielectric properties of living systems at both audio- and radio-frequencies change dramatically after death, we have suggested [5, 18] that the measurement of such properties might provide a novel, non-invasive and useful approach to the estimation of the time of death of a subject in forensic medicine, an estimation which is still subject to many uncertainties.

The distinction between life and non-life, albeit one that is not at all simple to make [124], is of course but one extreme subset of the variety of physiological states that a tissue may adopt. Many diagnostic techniques rely on dielectric properties, are summarised by Pethig and Kell [13] and Davey and Kell [18], and include [125, 126] electrical impedance tomography (see, e.g., refs. 127–132), and impedance plethysmography [133–138] and pneumography [139, 140]. The correlation between whole-body impedance and body composition, particularly adipose

tissue content, is now well-established (see, e.g., ref. 141). All of these, and other, techniques rely upon the dielectric behaviour described in the preceding sections.

### 5. Nonlinear interactions of cells with electrical fields

As was discussed above, the simplest type of dipolar billiard ball rotation results ultimately in the simple transduction of exogenous electrical energy, via mechanical (frictional) forces, into heat. However, Astumian, Westerhoff and their coworkers have shown that the properties required of an enzyme to "harvest" energy from an exogenous electrical field are common to all enzymes. These properties are possession of conformational states which possess different dipole moments and which interconvert *hierarchically* and in a fashion that is coupled to their chemical environment [81, 142–147]. In particular, it was shown that such energy converters *must* act nonlinearly, and it was argued that this might be visible as the conversion of the frequency of an exciting electrical field to another frequency [12, 30, 147–151]. This could be expected to occur at field strengths in which traditional measurements (of a voltage-independent impedance) would suggest that a purely linear system was being observed (Fig. 22).

In essence, this turns out to be a severe case of "rose-coloured spectacles" because of the fact that most impedimetric devices *assume* linearity, such measuring systems are normally so organised (electronically) that they reject currents at frequencies other than that of the

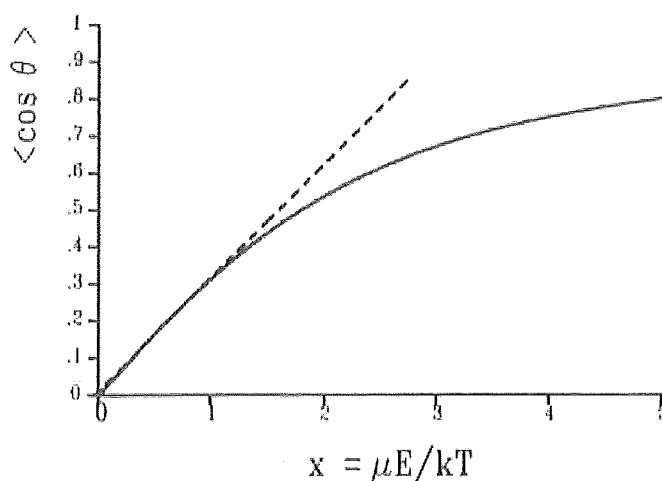


Fig. 22. The Langevin function. The ordinate represents the mean extent of orientation of an ensemble of randomly arrayed (electric) dipoles of dipole moment  $\mu$  as a function of the electric field strength  $E$ . The solid line is the Langevin function  $\langle \cos \theta \rangle = \coth x - 1/x$ , where  $x = \mu E/kT$ , whilst the dotted line indicates the domain of linearity in which the (displacement) current is proportional to the potential difference (field strength) applied.

exciting potential difference [5, 19]. Thus a system which may *appear* linear (in that the observable current is linear with the exciting potential difference) may in fact be nonlinear (in that the system causes what may be a constant fraction of the exciting potential difference to be transformed into currents at *other* than the exciting frequency). One system that has been widely discussed is referred to as the four-state enzyme.

## 6. A four-state enzyme capable of harvesting electrical energy for the performance of useful (bio)chemical work

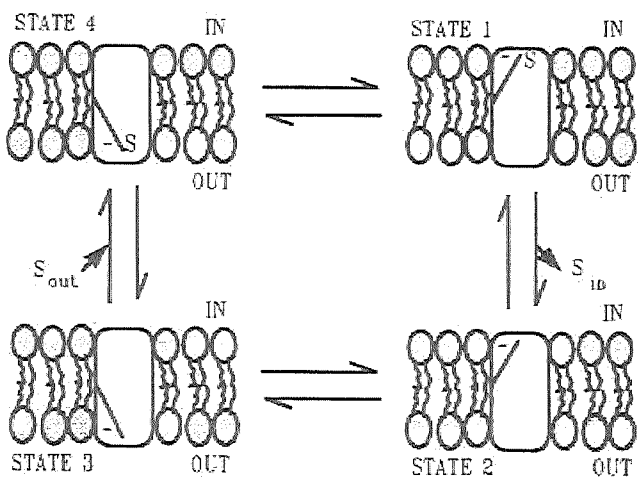
The average potential in a sinusoidally modulated field with no d.c. bias is zero. In most cases where it interacts with an aqueous system (and in accordance with this idea) it merely produces heat under macroscopically isothermal conditions. However, it certainly constitutes a source of *free* energy (as is evident from its ability to do such things as to drive a power drill). To provide a simple illustration of the properties of a system which does not merely turn this electric field energy into heat and which can therefore conserve this free energy as useful (electro)chemical work [149, 151], we discuss (Fig. 23) a four-state, membrane-located pump (which does not therefore rotate around an axis parallel to the membrane), capable of transporting an uncharged molecule (S) which is present at a higher concentration inside the cell than that outside in a direction opposite to its (electro)chemical potential.

The protein possesses a negatively charged binding site for S which can make transitions between the inner and outer faces of the membrane. (It is not necessary that it crosses the whole membrane, merely the region where the potential drop is the greatest.) The protein possesses, and cycles between, four conformational states (1 to 4), which represent the combination of bound or non-bound substrate with the negatively charged binding site facing either inwards or outwards. States 4 and 2 have lower basic free energies [28, 152] than states 1 and 3, and thus are more stable (i.e. highly populated). Cycling of the protein in a clockwise direction would have the effect of "pumping" S against its chemical potential, such that to effect this an exogenous source of free energy is necessary. In the absence of any field, therefore, and because of a higher affinity for its substrate than for any of the other states, state 4 is the most highly populated (Fig. 23A) in the ensemble of protein molecules.

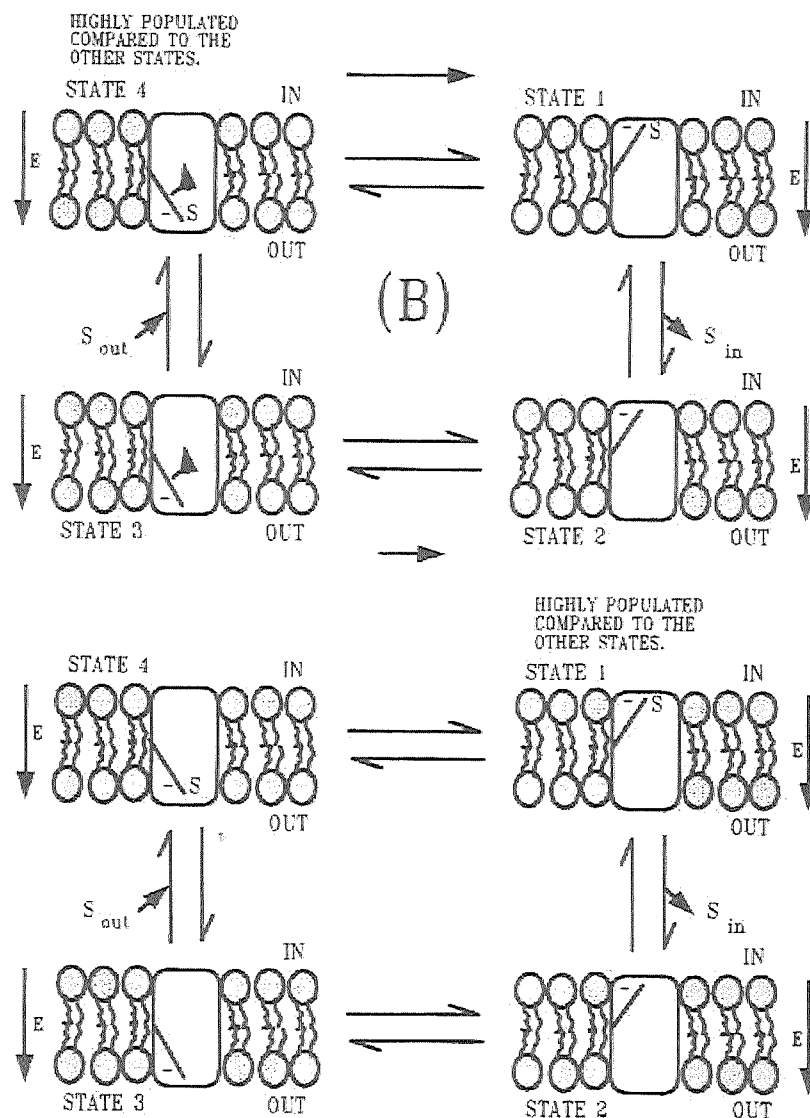
If one applies a "low-frequency" alternating field (whose frequency  $f < f_c$  for the  $\beta$ -dispersion, such that the membranes are charged up and a (fluctuating) membrane potential is induced), the protein will be oriented (say), during the first half-cycle, in a direction that attracts the negatively charged binding site towards the inner face of the membrane

(A)

HIGHLY POPULATED  
COMPARED TO THE  
OTHER STATES.



(B)



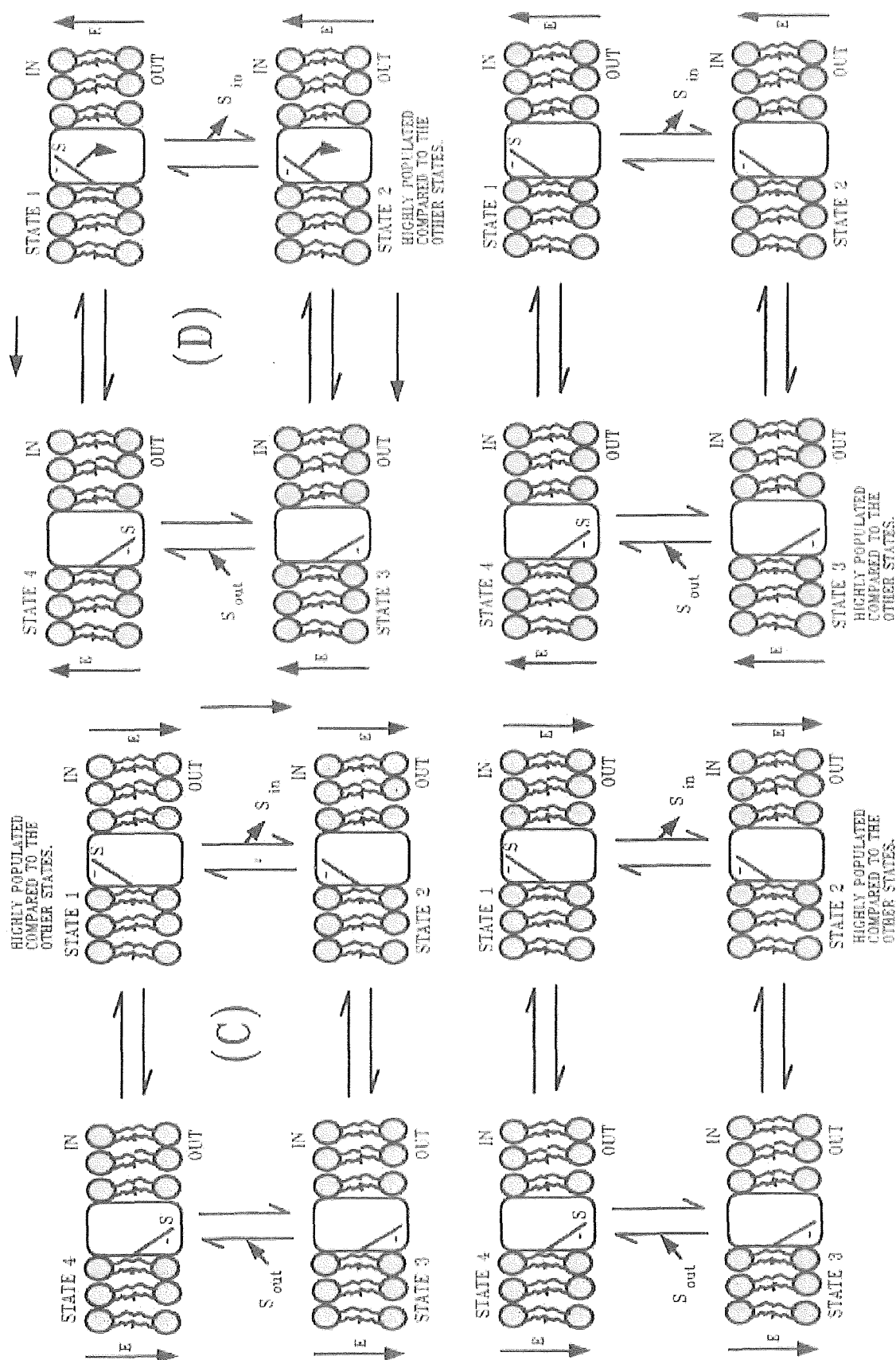


Fig. 23. The behaviour of a four-state enzyme in an alternating electrical field of a suitable frequency. For full discussion of this diagram, see the text.

(Fig. 23B). This effectively causes transitions from states  $4 \rightarrow 1$  and state  $3 \rightarrow 2$ . Thus state 1 will have become the most highly populated state and there will have been a net translocation of S from outside to inside. However, since state 2 also has its negative charge in the energetically favoured inner position, and since it also has a lower free energy than state 1, there will then be a re-equilibration between (the populations in) states 1 and 2 (Fig. 23C). Thus state 2 will become more highly populated than the other states, and because the transition  $1 \rightarrow 2$  releases S on the inside, there will be a net release of S to the cytoplasm.

When the second half of the a.c. field is applied, i.e. when the applied electric field is of the opposite polarity, the favoured position of the negatively charged binding site will now be at the outer face of the membrane. This will cause transitions from  $2 \rightarrow 3$  and from  $1 \rightarrow 4$ . The immediate result now is that state 3 becomes more populated than the outer states (Fig. 23D). In other words, there has been a net movement of empty binding sites from the inside to the outside of the membrane. However, since state 4 also has its negative charge in the energetically more favoured outside position, and has a lower free energy than does state 3, there is another re-equilibration, this time in the direction  $3 \rightarrow 4$ .

The net result of this, from the protein's point of view, is that one has returned to the starting position (Fig. 23A). In a sense, this is to be expected, since the net potential of the field was indeed zero. Yet despite this fact the field has done work on the system, since the clockwise cycling of the protein caused it to pump S against its electrochemical gradient and under macroscopically isothermal conditions. As discussed for instance by Welch and Kell [149], such transduction of non-stationary electric field energy and chemical energy does not violate the Second Law, but merely indicates that proteins are not simple dipolar billiard balls.

As indicated above, the properties required of the model four-state enzyme are common to all enzymes, viz. the possession of conformational states of different dipole moments which are coupled to each other in a hierarchical fashion, which possess different free energies and the transitions between which are therefore coupled to electr(ochem)ical reactions. Whilst this does not of itself indicate which enzymes one should seek to consider as the most likely or suitable "targets" for low-energy exogenous electrical fields, and the metabolic control analysis (for a recent review of which see refs. 152–154) indicates that there is rarely a "unique" target, the amplifying effects of membranes on electrical fields suggest that initial attention might most fruitfully be directed at membranous ones. Similarly, the fact that the exogenous field causes the re-equilibration of protein conformational states which have different dipole moments indicates that one might most expect to see field-induced currents at frequencies related to the turnover number of the enzyme in question.



It is worth mentioning here that harmonics have been observed experimentally (under conditions in which the fundamental *appears* linear) in a number of systems in which the electrical fields across the dielectric layer have been fairly high. Such systems include artificial polymers [155, 156], nerve axons [157–159], black lipid membranes [160, 161] and bilayer-modified electrodes [162, 163], consistent with the arguments developed herein and elsewhere [30, 147]. More recently, we have for the first time observed the generation of harmonics in *cell suspensions*, i.e. where the electrodes are not on either side of the dielectric “membrane” layer [164–166]. In this work, with resting suspensions of cells of yeast (*S. cerevisiae*), substantial third harmonics were generated in a field- and frequency-dependent fashion, with an optimal frequency of excitation of 15 to 20 Hz and an optimal field strength (judged from the electrode side of the electrode-electrolyte interface) of only 2 V/cm. Inhibitor studies (and later studies with mutant strains [204]) revealed that the major source of this nonlinear dielectricity was (interaction of the electric field with) the  $H^+$ -ATPase in the plasma membrane of these cells, whose turnover number  $k_{cat}$  is rather precisely that of the optimum frequency of excitation. When the cells were allowed to glycolyse, the odd-numbered harmonics were replaced by even-numbered (second and fourth) harmonics. If the cells were subjected to two-frequency excitation (i.e. with a waveform created by mixing the output from two sinusoidal generators), both exciting frequencies *cooperated* in the generation of frequencies other than those in the exciting waveform; with resting cells these were  $f_1 \pm 2f_2$  and  $f_2 \pm 2f_1$  whilst with glycolysing cells they were  $2f_1$ ,  $2f_2$  and  $f_1 + f_2$ . Nonlinear dielectricity was also observed in respiratory [205] and photosynthetic [206] bacteria, where the main source appeared to be enzymes in the membranous electron-transport chains of these organisms. All of these findings are consistent with the generalised properties of enzymes described above, and often referred to as “electroconformational coupling” [145–147]. Although this work to date has concentrated on the use of sinusoids, the *design* of optimal waveforms for interacting with particular targets does not in principle differ from the design of drugs aimed at selective interaction with appropriate targets or receptors [150]. It is clear that electrical measurements of these nonlinear properties provide a particularly *direct* and convenient means of assessing the ability (see, e.g., refs. 167–190) of weak electrical fields to exert biological activity.

## 7. Concluding remarks

The present survey has enabled us to review (i) the means by which we measure the dielectric properties of biological cell suspensions, (ii) the

manner in which we extract structural and molecular information from the macroscopic observables, and (iii) the state of our knowledge of the low-frequency, passive electrical properties of biological cells and their biophysical basis. Finally, we have provided an introduction to the recently recognised *nonlinear* electrical properties of biological cells, and have indicated, in these banal times, how one may use our hard-won knowledge of the dielectric properties of living cells for the development of novel and useful diagnostic and therapeutic devices.

### Acknowledgments

We would like to thank the Chemicals and Pharmaceuticals Directorate of the Biotechnology and Biological Sciences Research Council, U.K., the Wolfson Foundation, the Department of Trade and Industry, Aber Instruments and FT Applikon for support of our work on Biological Dielectrics.

### References

1. JT Stock, *Anal. Chem.* 56 (1984) 561A-570A.
2. H Fricke, *J. Gen. Physiol.* 9 (1925) 137-152.
3. AL Hodgkin and AF Huxley, *J. Physiol.* 117 (1952) 300-544.
4. ID Campbell and RA Dwek, *Biological Spectroscopy*, Benjamin-Cummings, London, 1984.
5. DB Kell and CL Davey in *Biosensors: a Practical Approach*, AEG Cass (ed), IRL Press, Oxford, 1990, pp. 125-154.
6. EH Grant, RJ Sheppard and GP South, *Dielectric Behaviour of Biological Molecules in Solution*, Clarendon Press, Oxford, 1978.
7. OF Schanne and ERP Ceretti, *Impedance Measurements in Biological Cells*, Wiley, New York, 1978.
8. R Pethig, *Dielectric and Electronic Properties of Biological Materials*, Wiley, Chichester, 1979.
9. U Zimmermann, *Biochim. Biophys. Acta* 694 (1982) 227-277.
10. DB Kell and CM Harris, *J. Bioelectricity* 4 (1985) 317-348.
11. KR Foster and HP Schwan in *C.R.C. Handbook of Biological Effects of Electromagnetic Fields*, C. Polk and E. Postow (eds), C.R.C. Press, Boca Raton, 1986, pp. 27-96.
12. DB Kell in *Biosensors: Fundamentals and Applications*, APF Turner, I Karube and GS Wilson (eds), Oxford University Press, Oxford, 1987, pp. 427-468.
13. R Pethig and DB Kell, *Phys. Med. Biol.* 32 (1987) 933-970.
14. DB Kell, *I.S.I. Atlas of Science: Biochemistry I* (1988) 25-29.
15. CL Davey and DB Kell in *Electric Field Phenomena in Biological Systems*, R Paris (ed), Institute of Physics, London, 1989, pp. 51-62.
16. KR Foster and HP Schwan, *C.R.C. Crit. Rev. Biomed. Eng.* 17 (1989) 25-102.
17. S Takashima, *Electrical Properties of Biopolymers and Membranes*, Adam Hilger, Bristol, 1989.
18. CL Davey and DB Kell in *Emerging Electromagnetic Medicine*, M O'Connor, R Bentall and JS Monahan (eds), Springer, Berlin, 1990, pp. 19-43.
- 18a. S Bone and B Zaba, *Bioelectronics*, Wiley, Chichester, 1992.
19. JR Macdonald, *Impedance Spectroscopy*, Wiley, New York, 1987.
20. R Pethig, *IEEE Trans. Electr. Insul.* EI-19 (1984) 453-474.
21. KS Cole and RH Cole, *J. Chem. Phys.* 9 (1941) 341-351.
22. B Hilezer and A Malecki, *Electrets*, Elsevier, Amsterdam, 1986.
23. AK Jonscher, *Dielectric Relaxation in Solids*, Chelsea Dielectrics Press, London, 1983.
24. L Dissado and RM Hill, *Proc. R. Soc. Ser. A* 390 (1983) 131-180.
25. RM Hill and AK Jonscher, *Contemp. Phys.* 24 (1983) 75-110.

26. HP Schwan, *Adv. Biol. Med. Phys.* 5 (1957) 147-209.
27. JB Hasted, *Aqueous Dielectrics*, Chapman and Hall, London, 1973.
28. TL Hill, *Free Energy Transduction in Biology*, Academic Press, New York, 1977.
29. AR Fersht, *Enzyme Structure and Mechanism*, 2nd Edition, Freeman, San Francisco, 1985.
30. DB Kell, RD Astumian and HV Westerhoff, *Ferroelectrics* 86 (1988) 59-78.
31. JR Macdonald and MK Brachman, *Rev. Mod. Phys.* 28 (1956) 393.
32. P Debye, *Polar Molecules*, Dover Press, New York, 1929.
33. JL Oncley in *Proteins, Amino Acids and Peptides*, FJ Cohn and JT Edsall (eds), Reinhold, New York, 1943.
34. DJ Barlow and JM Thornton, *Biopolymers* 25 (1986) 1717.
35. JG Kirkwood, *J. Phys. Chem.* 2 (1932) 351.
36. DB Kell, *Bioelectrochem. Bioenerg.* 15 (1983) 405-415.
37. DB Kell and CM Harris, *Eur. Biophys. J.* 12 (1985) 181-197.
38. CM Harris and DB Kell, *Eur. Biophys. J.* 13 (1985) 11-24.
39. HP Schwan in *Physical Techniques in Biological Research*, WL Nastuk (ed), Academic Press, New York, 1963, Vol. VI B, pp. 323-407.
40. CL Davey, GH Markx and DB Kell, *Eur. Biophys. J.* 18 (1990) 255-265.
41. J Barber, *Annu. Rev. Pl. Physiol.* 33 (1982) 261-295.
42. AM James, *Adv. Coll. Interf. Sci.* 15 (1982) 171-221.
43. S McLaughlin, *Annu. Rev. Biophys. Chem.* 18 (1989) 113-136.
44. RY Stainer, EA Adelberg and JL Ingraham, *General Microbiology*, 4th Edition, Macmillan, London, 1984.
45. G Schwarz, *J. Phys. Chem.* 66 (1962) 2636-2642.
46. CW Einolf (Jr.) and EL Carstensen, *Biophys. J.* 13 (1973) 8-13.
47. CW Einolf (Jr.) and EL Carstensen, *J. Phys. Chem.* 75 (1971) 1091-1099.
48. HP Schwan and HJ Morowitz, *Biophys. J.* 2 (1962) 395-340.
49. EL Carstensen, HA Cox (Jr.), WB Mercer and LA Natale, *Biophys. J.* 5 (1965) 289-300.
50. EL Carstensen, *Biophys. J.* 7 (1967) 493-503.
51. EL Carstensen and RE Marquis, *Biophys. J.* 8 (1968) 536-548.
52. CW Einolf (Jr.) and EL Carstensen, *Biophys. J.* 9 (1969) 634-643.
53. EL Carstensen, J. Maniloff and CW Einolf (Jr.), *Biophys. J.* 11 (1971) 572-581.
54. EL Carstensen and RE Marquis in *Spores VI*, P Gerhardt, RN Costilow and HL Sadoff (eds), American Society for Microbiology, Washington, 1975, pp. 563-571.
55. LE Ferris, CL Davey and DB Kell, *Eur. Biophys. J.* 18 (1990) 267-276.
56. DB Kell, P John and SJ Ferguson, *Biochem. J.* 174 (1978) 257-266.
57. Y Sugura, S. Koga and H. Akabori, *J. Gen. Appl. Microbiol.* 10 (1964) 163-174.
58. K Asami, T Hanai and N Koizumi, *J. Membr. Biol.* 28 (1976) 169-180.
59. K Asami, *Bull. Inst. Chem. Res., Kyoto Univ.* 55 (1977) 394-414.
60. K Asami, T Hanai and N Koizumi, *J. Membr. Biol.* 34 (1977) 145-156.
61. CM Harris and DB Kell, *Bioelectrochem. Bioenerg.* 11 (1983) 15-28.
62. A Irimajiri, Y Doida, T Hanai and A Inouye, *J. Membr. Biol.* 38 (1978) 209-232.
63. A Surowiec, S Stuchly and C Izaguirre, *Phys. Med. Biol.* 31 (1986) 43-53.
64. A Irimajiri, K Asami, T Ichinowatari and Y Kinoshita, *Biochim. Biophys. Acta* 896 (1987) 203-213.
65. CL Davey, DB Kell, RB Kemp and RWJ Meredith, *Bioelectrochem. Bioenerg.* 20 (1988) 83-98.
66. HP Schwan and TP Bothwell, *Nature* 178 (1956) 265-267.
67. HP Schwan and EL Carstensen, *Science* 125 (1957) 985-986.
68. HP Schwan, *Blut* 46 (1983) 185-197.
69. E Ponder and RV Ponder, *Exp. Biol.* 32 (1955) 175-182.
70. DH Heard and DVH Seamen, *J. Gen. Physiol.* 43 (1960) 635-654.
71. SS Dukhin and VN Shilov, *Dielectric Phenomena and the Double Layer in Disperse Systems and Polyelectrolytes*, Wiley, Chichester, 1974.
72. RW O'Brien, *Adv. Coll. Interf. Sci.* 16 (1982) 281-320.
73. P Fatt, *Proc. R. Soc. Ser. B* 159 (1964) 606-651.
74. G Falk and P Fatt, *Proc. R. Soc. Ser. B* 160 (1964) 69-123.
75. M Mandel, *Ann. N.Y. Acad. Sci.* 74 (1977) 303-311.

76. S Takashima, C Gabriel, RJ Sheppard and EH Grant, *Biophys. J.* 54 (1984) 995.
77. K Lim and El Franes, *J. Coll. Interf. Sci.* 110 (1986) 201-213.
78. H Pauly, *IRE Trans. Biomed. Electron.* 9 (1962) 93-95.
79. U Zimmermann, *Trends Biotechnol.* 1 (1983) 149-155.
80. E Neumann in *Modern Bioelectrochemistry*, F Gutmann and H Keyzer (eds), Plenum Press, New York, 1986, pp. 97-132.
81. TY Tsong and RD Astumian, *Bioelectrochem. Bioenerg.* 15 (1986) 457.
82. H Fricke, *Phys. Rev.* 26 (1925) 678-681.
83. A Irimajiri, T Hanai and A Inouye, *J. Theoret. Biol.* 78 (1979) 251-269.
84. K Asami, T Hanai and N Koizumi, *Biophys. J.* 31 (1980) 215-225.
85. S Velick and M Gorin, *J. Gen. Physiol.* 23 (1940) 753-771.
86. H Fricke, *J. Appl. Phys.* 24 (1953) 644-646.
87. H Fricke, *J. Phys. Chem.* 59 (1955) 168-170.
88. K Asami, T Hanai and N Koizumi, *Jap. J. Appl. Phys.* 19 (1980) 359-365.
89. KS Cole, *Membranes, Ions and Impulses*, University of California Press, Berkeley, 1972.
90. T Hanai, K Asami and N Koizumi, *Bull. Inst. Chem. Res. Kyoto Univ.* 57 (1979) 297-305.
- 90a. CL Davey, HM Davey and DB Kell, *Bioelectrochem. Bioenerg.* 28 (1992) 319-340.
91. CM Harris and DB Kell, *Biosensors* 1 (1985) 17-84.
92. CM Harris, RW Todd, SJ Bungard, RW Lovitt, JG Morris and DB Kell, *Enz. Micr. Technol.* 9 (1987) 181-186.
93. DB Kell, GH Markx, CL Davey and RW Todd, *Trends Anal. Chem* 9 (1990) 190-194.
94. GH Markx and DB Kell, *Biofouling* 2 (1990) 211.
95. GH Markx, CL Davey and DB Kell, *J. Gen. Microbiol.* 137 (1991) 735-743.
96. GH Markx, CL Davey and DB Kell, *Bioelectrochem. Bioenerg.* 25 (1991) 195-211.
97. CL Davey, W. Peñaloza, DB Kell and JN Hedger, *World J. Microbiol. Biotechnol.* 7 (1991) 248-259.
98. W. Peñaloza, CL Davey, JN Hedger and DB Kell, *World J. Microbiol. Biotechnol.* 7 (1991) 260-268.
- 98a. R Fehrenbach, M Comberbach and JO Petre, *J. Biotechnol.* 23 (1992) 303-314.
99. BA Adams, *J. Exp. Biol.* 133 (1987) 169-182.
100. Rothschild, J. *Biophys. Biochem. Cytol.* 3 (1956) 103-109.
101. A Irimajiri, K Asami, T Ichinowatari and Y Kinoshita, *Biochim. Biophys. Acta* 896 (1987) 214.
102. DW Tempest, *Symp. Soc. Gen. Microbiol.* 19 (1969) 87-111.
103. H Pauly and HP Schwan, *Biophys. J.* 6 (1966) 621-639.
104. HM Shapiro, *Practical Flow Cytometry*, 2nd Edition, Alan R. Liss, New York, 1988.
105. MR Melamed, PF Mullancy and ML Mendelsohn, *Flow Cytometry and Sorting*, Wiley, New York, 1979.
106. CL Davey, NM Dixon and DB Kell, *Binary* 2 (1990) 119-125.
107. CL Davey, DB Kell and NM Dixon, *Binary* 2 (1990) 127-132.
108. A Irimajiri, T Hanai and A Inouye, *Biophys. Str. Mech.* 1 (1975) 273-283.
109. K Sekine, T Hanai and N Koizumi, *Bull. Inst. Chem. Res. Kyoto Univ.* 61 (1983) 299-313.
110. CA Boulton, PS Maryan and D Loveridge, *Proc. 22nd Eur. Brewing Convention, Zürich* (1989) 653-661.
111. NG Stoicheva, CL Davey, GH Markx and DB Kell, *Biocatalysis* 2 (1989) 245-255.
- 111a. CL Davey, GH Markx and DB Kell, *Pure and Appl. Chem.* 65 (1993) 1921-1926.
112. H Fricke and HJ Curtis, *J. Gen. Physiol.* 18 (1935) 821-836.
113. H Pauly and HP Schwan, *IEEE Trans. Biomed. Eng. BME-11* (1964) 103-109.
114. Y Sugiura and S. Koga, *Biophys. J.* 5 (1965) 439-445.
115. EL Carstensen and RW Smearing, *IEEE Trans. Biomed. Eng. BME-14* (1967) 216-222.
116. H Morgan, M Ginzburg and BZ Ginzburg, *Biochim. Biophys. Acta* 924 (1987) 54-66.
117. V Lap, F Pliquett and U. Katenkamp, *Bioelectrochem. Bioenerg.* 17 (1987) 81-87.
118. F Pliquett and S. Wunderlich, *Studia Biophys.* 134 (1989) 73-76.
119. H Coster, DR Iyer and JR Smith in *Bioelectrochemistry*, H. Keyzer and F. Gutmann (eds), Plenum, New York, 1980, pp. 331-352.
120. E Perez and J Wolfe, *Eur. Biophys. J.* 16 (1988) 23-29.
121. F. Pliquett, *Bioliz.* 18 (1973) 1182-1185.

122. HJ Swatland, *J. Animal Sci.* 51 (1980) 1108–1112.
123. HP Schwan in *Biological Effects and Dosimetry of Nonionizing Radiation*, M. Grandolfo, SM Michaelson and A Rindi (eds), Plenum Press, New York, 1983, pp. 195–211.
124. L Watson, *The Romeo Error*, Hodder and Stoughton, 1974.
125. MF Iskander and AH Durney, *Proc. IEEE* 68 (1980) 126–132.
126. JP Grant and NM Spyrou, *J. Bioelectricity* 4 (1985) 419–458.
127. LR Pryce, *IEEE Trans. Nucl. Sci.* NS-26 (1979) 2736–2739.
128. RS Eisenberg and RT Mathias, *C.R.C. Crit. Rev. Bioeng.* 4 (1980) 203–232.
129. DC Barber and BH Brown, *J. Phys. E, Sci. Instr.* 17 (1984) 1–27.
130. T Murai and Y Kagawa, *IEEE Trans. Biomed. Eng.* BME-32 (1985) 177–184.
131. Anon, *Clin. Phys. Physiol. Meas.* 8, Suppl. A (1987) 181–184.
132. JC Newell, DG Gisser and D Isaacson, *IEEE Trans. Biomed. Eng.* BME-35 (1988) 828–833.
133. DW Hill in *Non-invasive Physiological Measurements*, P. Rolfe (ed), Academic Press, London, 1979.
134. SN Mohapatra, *Noninvasive Cardiac Monitoring by Electrical Impedance Technique*, Pitman, London, 1981.
135. HB Wheeler and NC Penney in *Noninvasive Diagnostic Techniques in Vascular Disease*, CV Bernstein (ed), Mosby, St Louis, 1982.
136. BH Brown in *Imaging with Nonionising Radiation*, DF Jackson (ed), Surrey University Press, Guildford, 1983, pp. 85–110.
137. FA Anderson (Jr.), *Ann. Biomed. Eng.* 12 (1984) 79–102.
138. DC Penney, *C.R.C. Crit. Rev. Biomed. Eng.* 13 (1986) 227–281.
139. RP Henderson and JG Webster, *IEEE Trans. Biomed. Eng.* BME-25 (1978) 250–254.
140. LE Baker in *Noninvasive Physiological Measurement*, P. Rolfe (ed), Academic Press, London, 1979.
141. RF Kushner, A. Kunigk, M. Alspaugh, PT Andronis, CA Leitch and DA Seocler, *Amer. J. Clin. Nutr.* 52 (1990) 219.
142. HV Westerhoff, TY Tsong, PB Chock, Y Chen and RD Astumian, *Proc. Natl. Acad. Sci.* 83 (1986) 4734–4738.
143. RD Astumian, PB Chock, TY Tsong, Y Chen and HV Westerhoff, *Proc. Natl. Acad. Sci.* 84 (1987) 434–438.
144. TY Tsong and RD Astumian, *Progr. Biophys. Mol. Biol.* 50 (1987) 1–45.
145. TY Tsong and RD Astumian, *Annu. Rev. Physiol.* 50 (1988) 273–290.
146. HV Westerhoff, DB Kell and RD Astumian, *J. Electrostatics* 21 (1988) 257–298.
147. HV Westerhoff, RD Astumian and DB Kell, *Ferroelectrics* 86 (1988) 79–101.
148. RD Astumian and B Robertson, *J. Chem. Phys.* 91 (1989) 4891.
149. GR Welch and DB Kell in *The Fluctuating Enzyme*, GR Welch (ed), Wiley, New York, 1986, p. 451.
150. DB Kell, *Univ. Wales Rev. Sci. Technol.* 1 (1988) 64.
151. DB Kell in *Biological Coherence and Response to External Stimuli*, H. Fröhlich (ed), Springer, Heidelberg, 1988, p. 233.
152. HV Westerhoff and K. van Dam, *Thermodynamics and Control of Biological Free-energy Transduction*, Elsevier, Amsterdam, 1987.
153. DB Kell, K van Dam and HV Westerhoff, *Symp. Soc. Gen. Microbiol.* 44 (1989) 61–93.
154. A Cornish-Bowden and M Cardenas (eds), *Control of Metabolic Processes*, Plenum Press, New York, London, 1990.
155. T Furukawa, K Nakajima, T Koizumi and M Date, *Jpn. J. Appl. Phys.* 26 (1987) 1039–1045.
156. T Furukawa, M Tada, K Nakajima and I. Seo, *Jap. J. Appl. Phys.* 27 (1988) 200–204.
157. LJ DeFelice, WJ Adelman (Jr.), DE Clapham and A Mauro in *The Biophysical Approach to Excitable Membranes*, WJ Adelman (Jr.) and De Goldman (eds), Plenum, New York, 1981, p. 37.
158. S Miyamoto and HM Fishman, *IEEE Trans. Biomed. Eng.* BME-33 (1986) 644–653.
159. HM Fishman, HR Leuchtag and LE Moore, *Biophys. J.* 43 (1983) 293.
160. W Carius, *J. Coll. Interf. Sci.* 57 (1976) 301.
161. VS Sokolov and VG Kuz'min, *Biofiz.* 25 (1980) 170.
162. K Yoshikawa, M. Shoji, S Nakata and S Maeda, *Langmuir* 4 (1988) 759.
163. S Nakata, K Yoshikawa, M Shoji, H Kawakami and T Ishii, *Biophys. Chem.* 34 (1989) 201.

164. A Woodward and DB Kell, *Bioelectrochem. Bioenerg.* 24 (1990) 83–100.
165. A Woodward and DB Kell, *Bioelectrochem. Bioenerg.* 25 (1991) 395–413.
166. DB Kell and A Woodward in *Proc. 4th BTK Meeting (Amsterdam)*, HV Westerhoff (ed), Intercept, London, 1991.
167. HS Burr, *Blueprint for Immortality*, Neville Spearman, London, 1977.
168. AS Presman, *Electromagnetic Fields and Life*, Plenum Press, New York, 1970.
169. AR Sheppard and M Eisenbud (eds), *Biological Effects of Electric and Magnetic Fields of Extremely Low Frequency*, New York University Press, New York, 1977.
170. H Fröhlich, *Adv. Electron. Electron Phys.* 53 (1980) 85.
171. WR Adey, *Physiol. Rev.* 61 (1981) 435–514.
172. KI Illinger (ed), *Biological Effects of Non-Ionising Radiation*, American Chemical Society, Washington, 1981.
173. HL König, AP Krueger, S Lane and W Sonniq, *Biological Effects of Environmental Electromagnetism*, Springer, Heidelberg, 1981.
174. RO Becker and AA Marino, *Electromagnetism and Life*, State University of New York Press, Buffalo, 1982.
175. H Fröhlich and F Kremer (eds), *Coherent Excitations in Biological Systems*, Springer, Heidelberg, 1983.
176. M Grandolfo, SM Michaelson and A Rindi (eds), *Biological Effects and Dosimetry of Nonionizing Radiation*, Plenum Press, New York, 1983.
177. MJ Allen and PNR Usherwood (eds), *Charge and Field Effects in Biosystems*, Abacus Press, Tunbridge Wells, 1984.
178. WR Adey and AF Lawrence (eds), *Nonlinear Electrodynamics of Biological Systems*, Plenum Press, New York, 1984.
179. A Chiabrera, C Nicolini and HP Schwan (eds), *Interactions between Electromagnetic Fields and Cells*, Plenum Press, New York, 1985.
180. DB Kell and HV Westerhoff in *Organised Multienzyme Systems: Catalytic Properties*, GR Welch (ed), Plenum Press, New York, 1985, pp. 63.
181. AA Marino and J Ray, *The Electric Wilderness*, University of San Francisco Press, San Francisco, 1986.
182. R Nuccitelli (ed), *Ionic Currents in Development*, Alan R Liss, New York, 1986.
183. C Polk and E Postow (eds), *C.R.C. Handbook of Biological Effects of Electromagnetic Fields*, C.R.C. Press, Boca Raton, 1986.
184. J Black, *Electrical Stimulation; its Role in Growth, Repair and Remodeling of the Musculoskeletal System*, Praeger, New York, 1987.
185. M Blank and A Findl (eds), *Mechanistic Approaches to Interaction of Electric and Magnetic Fields with Living Systems*, Plenum Press, New York, 1987.
186. H Fröhlich (ed), *Biological Coherence and Response to External Stimuli*, Springer, Heidelberg, 1988.
187. AA Marino, *Modern Bioelectricity*, Plenum Press, New York, 1988.
188. JC Lin (ed), *Electromagnetic Interaction with Biological Systems*, Plenum Press, New York, 1989.
189. CW Smith and S Best, *Electromagnetic Man*, Dent, London, 1990.
190. JC Weaver and RD Astumian, *Science* 247 (1990) 459.
191. RA Charman, *Physiotherapy* 76 (1990) 502.
192. H Fricke, *Nature* 172 (1953) 731–732.
193. W Jaroszynski, J Terlecki, A Mysliwski, J Misiowska and J Witkowski, *Fol. Histochem. Cytochem.* 21 (1983) 161–172.
194. W Jaroszynski, J Terlecki and J Sulocki, *Studia Biophys.* 107 (1985) 117–126.
195. C Ballario, A Bonincontro, C Cametti, A Rosi and I. Sportelli, *Z. Naturforsch.* 39C (1984) 160–166.
196. H Fricke and HJ Curtis, *Nature* 134 (1934) 102–103.
197. S Takashima and HP Schwan, *J. Membr. Biol.* 17 (1974) 51–68.
198. S Takashima, K Asami and Y Takahashi, *Biophys. J.* 54 (1989) 995.
199. K Asami, Y Takahashi and S Takashima, *Biochim. Biophys. Acta* 1010 (1989) 49–55.
200. H Pauly, *Nature* 183 (1959) 333–334.
201. I Bielińska and J Terlecki, *Fol. Histochem. Cytobiol.* 23 (1985) 33–42.
202. S Bantembach and J Terlecki, *Post. Fiz. Med.* 15 (1980) 87–95.
203. AA Laogun, *J. Bioelectricity* 5 (1986) 129–137.

204. A Woodward and DB Kell, *F.E.M.S. Microbiol. Let.* 84 (1991) 91–96.  
 205. A Woodward and DB Kell, *Bioelectrochem. Bioenerg.* 26 (1991) 423–439.  
 206. A McShea, A Woodward and DB Kell, *Bioelectrochem. Bioenerg.* 29 (1992) 205–214.

## Appendix A. Glossary

SI units of quantities are given in parenthesis.

$\alpha$	the Cole-Cole $\alpha$ is a dimensionless quantity used in the Cole-Cole equations
$a$	the radius of a spherical protein (m)
$A$	the area of each electrode in a plane-parallel electrode system ( $\text{m}^2$ )
$B$	susceptance of a system (S)
$c$	protein concentration ( $\text{kg m}^{-3}$ )
$C$	the admittance domain capacitance (F)
$C'$	the impedance domain capacitance (F)
$C_m$	membrane capacitance per unit membrane area ( $\text{F m}^{-2}$ )
$d$	the distance between the electrodes of a plane-parallel electrode (m)
$\Delta\epsilon'$	the relative permittivity (or dielectric) increment of a dispersion. This is the magnitude of the change in relative permittivity during a given dispersion
$\Delta\sigma'$	the conductivity increment of a dispersion ( $\text{S m}^{-1}$ ). This is the magnitude of the change in conductivity during a given dispersion
$\Delta\varphi_m$	induced membrane potential (V)
$\xi$	molecular friction coefficient
$\epsilon_0$	permittivity of free space, is the capacitance of a unit cell containing a vacuum, and equal to $8.854 \times 10^{-12} \text{ F m}^{-1}$
$\epsilon'_t$	the real part of the relative permittivity
$\epsilon'_{th}$	the limiting relative permittivity at frequencies high with respect to a given dispersion
$\epsilon'_i$	the relative permittivity of the inside (cytoplasm) of biological cells
$\epsilon'_{il}$	the limiting relative permittivity at frequencies low with respect to a given dispersion
$\epsilon'_{\omega}$	relative permittivity at a given (angular) frequency
$\epsilon''_t$	the imaginary part of the relative permittivity
$\epsilon''_{\omega}$	the imaginary part of the relative permittivity at a given (angular) frequency
$\epsilon^*_{\omega}$	the complex relative permittivity at a given (angular) frequency
$E$	electric field strength ( $\text{V m}^{-1}$ )

$E_0$	applied exogenous field strength ( $\text{V m}^{-1}$ )
$f$	frequency in (Hz)
$f_1$	output frequency of the first of a pair of sinusoidal generators (Hz)
$f_2$	output frequency of the second of a pair of sinusoidal generators (Hz)
$f_c$	the frequency when the fall in permittivity (or rise in conductivity) during a dispersion is half completed (Hz). This frequency is called either the critical or characteristic frequency of the dispersion
$f_{c,\epsilon}$	the frequency when the fall in permittivity during a dispersion is half completed (Hz)
$f_{c,\sigma}$	the frequency when the rise in conductivity during a dispersion is half completed (Hz)
$g$	a parameter used to account for molecular associations
$G$	the (admittance domain) conductance (S)
$i$	the square root of $-1$
$I_m$	the amplitude of the sinusoidal current flowing in a system (A)
$k$	Boltzmann's constant
$k_{\text{cat}}$	enzyme turnover number ( $\text{S}^{-1}$ )
$M$	the molecular weight of a protein
$\eta$	the viscosity of the medium in which a protein is suspended ( $\text{kg m}^{-1} \text{s}^{-1}$ )
$N$	Avogadro's number
$\theta$	used to represent angles
$P$	volume fraction of biological cells
$Q$	charge (C)
$Q_i$	counterion charge (C)
$r$	radius of a colloidal particle or biological cell (m)
$R$	admittance domain resistance ( $\Omega$ )
$R'$	impedance domain resistance ( $\Omega$ )
$s$	the distance between the charges at opposite ends of a dipole (m)
$\sigma'$	conductivity ( $\text{S m}^{-1}$ )
$\sigma'_h$	the limiting conductivity at frequencies high with respect to a given dispersion ( $\text{S m}^{-1}$ )
$\sigma'_i$	the conductivity of the inside (cytoplasm) of biological cells ( $\text{S m}^{-1}$ )
$\sigma'_l$	the limiting conductivity at frequencies low with respect to a given dispersion ( $\text{S m}^{-1}$ )
$\sigma'_o$	the conductivity of the medium in which biological cells are suspended ( $\text{S m}^{-1}$ )
$\sigma'_\omega$	the conductivity at a given (angular) frequency ( $\text{S m}^{-1}$ )
$t$	time (s)
$\tau$	the relaxation time of a dispersion (s)



T	absolute temperature (K)
u	the surface mobility of the counterions around colloidal particles
U	applied potential difference (V)
$U_m$	the amplitude of the sinusoidal potential difference applied to a system (V)
$\mu$	the (electric) dipole moment (C m; for historical reasons, dipole moments are often given in the non-SI unit Debye (D), where $1 \text{ D} = 3.33 \times 10^{-30} \text{ C m}$ )
$\omega$	the angular frequency (radians/s)
X	reactance ( $\Omega$ )
Y	admittance (S)
Z	the (complex) impedance ( $\Omega$ )
$Z'$	the real part of the complex impedance = $R'$ ( $\Omega$ )
$Z''$	the imaginary part of the complex impedance = $-X$ ( $\Omega$ )